not further reduce their body temperatures under the fed condition (Figure 3I, left panel). We next examined the effect of cold exposure on 24 hr fasted mice. Unlike with 48 hr fasting, under 24 hr fasting conditions, *AceCS2*$^{-/-}$ mice maintained their core body temperatures at levels similar to *AceCS2*$^{+/+}$ mice, although both levels were equally reduced by 2°C–3°C compared to fed levels. Exposure of these mice to cold further decreased their core temperatures; however, after 5 hr cold exposure, there was no significant difference between *AceCS2*$^{-/-}$ and *AceCS2*$^{+/+}$ mice (Figure 3I, right panel). These data indicate that adaptive thermogenesis in response to low temperature was not impaired in *AceCS2*$^{-/-}$ mice and further suggest that the sympathetic nervous system is able to properly maintain core body temperature in *AceCS2*$^{-/-}$ mice.

We hypothesized that fasting *AceCS2*$^{-/-}$ mice would lead to decreased exercise tolerance, owing to impaired acetate oxidation and subsequent reduction of ATP production in skeletal muscle (Figure 3E). *AceCS2*$^{-/-}$ mice were exercised on a motorized treadmill apparatus using a run-to-exhaustion protocol. *AceCS2*$^{-/-}$ mice fasted for 48 hr exhibited a markedly reduced capacity to sustain running exercise, whereas the running capacity of *AceCS2*$^{+/+}$ mice did not change between the fed and fasted conditions (Figure 3J). This suggests that acetate is an important fuel required for exercise as well as for heat generation during fasting.

### *AceCS2*$^{-/-}$ Mice Compensate for Metabolic Acidosis through Hyperventilation

Because the plasma acetate levels are very high in *AceCS2*$^{-/-}$ mice, we speculated that these mice could be acidotic, and, if not, they might be hyperventilating to blow off $CO_2$ to prevent acidemia. Accordingly, we measured the arterial blood gases, pH, and bicarbonate concentration. The values of arterial carbon dioxide partial pressure ($PaCO_2$) were significantly decreased in *AceCS2*$^{-/-}$ mice ($p < 0.05$, n = 5–6), indicating that *AceCS2*$^{-/-}$ mice were hyperventilating to blow off $CO_2$. There were no significant differences in the values of $PaO_2$, standardized bicarbonate concentration ($[HCO_3^-]$), and the pH (Table 1). These data indicate that *AceCS2*$^{-/-}$ mice were hyperventilating to compensate for a possible acidosis caused by acetate accumulation. This hyperventilation in *AceCS2*$^{-/-}$ mice might account for some of their increased energy expenditure compared to *AceCS2*$^{+/+}$ mice.

### *AceCS2*$^{-/-}$ Mice Exhibit Hypothermia and Hypoglycemia under Low-Carbohydrate, High-Fat Diet

Similar to fasting conditions, we hypothesized that acetate utilization may be important under low-glucose or low-carbohydrate intake states. To examine this possibility, 4-week-old *AceCS2*$^{-/-}$ and *AceCS2*$^{+/+}$ mice were fed a low-carbohydrate, high-fat diet (LC/HF; 0.4% carbohydrate, 90.5% fat, and 9.1% protein from calories). At the time of weaning (4 weeks of age), *AceCS2*$^{-/-}$ mice weighed an average of 40% less than their littermates (Figures S1A–S1C), and plasma acetate levels were markedly elevated (Figure 4A). Plasma ketone bodies, NEFA, glucose, and insulin levels were comparable between *AceCS2*$^{+/+}$ and *AceCS2*$^{-/-}$ mice (Table S1).

On LC/HF diet, *AceCS2*$^{-/-}$ mice exhibited lower body temperatures (Figure 4B). This was most severe (30.1 ± 1.4°C) on day 2 of LC/HF diet feeding, whereas *AceCS2*$^{+/+}$ mice maintained their body temperatures at 37°C on this diet. In addition, *AceCS2*$^{-/-}$ mice lost weight, whereas the body weight of *AceCS2*$^{+/+}$ mice remained stable (Figure 4C). Furthermore, *AceCS2*$^{-/-}$ mice had sustained hypoglycemia (56 ± 5 mg/dl) over this period compared to *AceCS2*$^{+/+}$ mice that exhibited transiently decreased plasma glucose levels at weaning but soon recovered to normal levels (137 ± 7 mg/dl) (Figure 4D). This transient hypoglycemia in *AceCS2*$^{+/+}$ is most likely from the stress of forced weaning, which causes suppression of feeding on the day of weaning. Plasma NEFA and ketone body levels were highly elevated, but there were no significant differences between *AceCS2*$^{+/+}$ and *AceCS2*$^{-/-}$ mice except in ketone body levels on day 3 of the LC/HF diet (Figures 4E and 4F). The abundance of mRNAs for the enzymes involved in gluconeogenesis was not decreased in *AceCS2*$^{-/-}$ mice compared to *AceCS2*$^{+/+}$ mice (Figure S3A). Furthermore, injection of pyruvate to these mice rescued hypoglycemia (Figure S3B), indicating that the gluconeogenic pathway is intact.

**Table 1. Blood Gas Analysis of *AceCS2*$^{+/+}$ and *AceCS2*$^{-/-}$ Mice**

| | +/+ | −/− |
|---|---|---|
| pH | 7.34 ± 0.03 | 7.34 ± 0.03 |
| $PaO_2$ (mm Hg) | 102.3 ± 2.7 | 108.8 ± 5.5 |
| $PaCO_2$ (mm Hg) | 37.3 ± 1.2 | 33.3 ± 0.9[a] |
| $HCO_3^-$ (mM) | 19.7 ± 0.8 | 17.6 ± 1.3 |
| BE (mM) | −5.1 ± 1.2 | −6.9 ± 1.9 |

Male mice (12 weeks old, n = 6 per genotype) were fed on a normal chow diet. Samples were obtained from the femoral artery of awake, freely moving mice. Data are mean ± SEM.
[a] $p < 0.05$ compared to *AceCS2*$^{+/+}$.

After 5 days of LC/HF diet feeding, *AceCS2*$^{-/-}$ mice began to die, and, by 21 days, 50% of the *AceCS2*$^{-/-}$ mice had died. By contrast, none of *AceCS2*$^{+/+}$ mice died (Figure 4G). However, following 21 days on the LC/HF diet, the surviving *AceCS2*$^{-/-}$ mice gradually recovered body temperature and plasma glucose levels. We observed no further excess mortality (data not shown).

Weight, body temperature, and plasma parameters (glucose, NEFA, and ketone bodies) did not differ significantly between the *AceCS2*$^{-/-}$ mice that died and those that survived during the 4 day period of LC/HF feeding after the weaning (Figures S4A–S4E). Therefore, the cause of death was not simply from malnutrition. We also examined the effect of a high-carbohydrate, high-fat (HC/HF) diet (58% fat, 15% protein, and 27% carbohydrate from calories). On this diet, both *AceCS2*$^{-/-}$ and *AceCS2*$^{+/+}$ mice survived with no deaths (data not shown). These data indicated that acetate oxidation mediated by AceCS2 is essential to maintain normal thermogenesis and fuel usage under low-glucose utilization states such as low-carbohydrate diets or fasting.

### *AceCS2*$^{-/-}$ Mice Exhibit Low Body Weight Gain under Low Carbohydrate Intake

We continued to feed the surviving *AceCS2*$^{-/-}$ mice an LC/HF diet. *AceCS2*$^{+/+}$ mice fed on this diet gained weight efficiently; by contrast, *AceCS2*$^{-/-}$ mice exhibited reduced weight gain under this diet (Figure 5A). Food intake was unchanged between

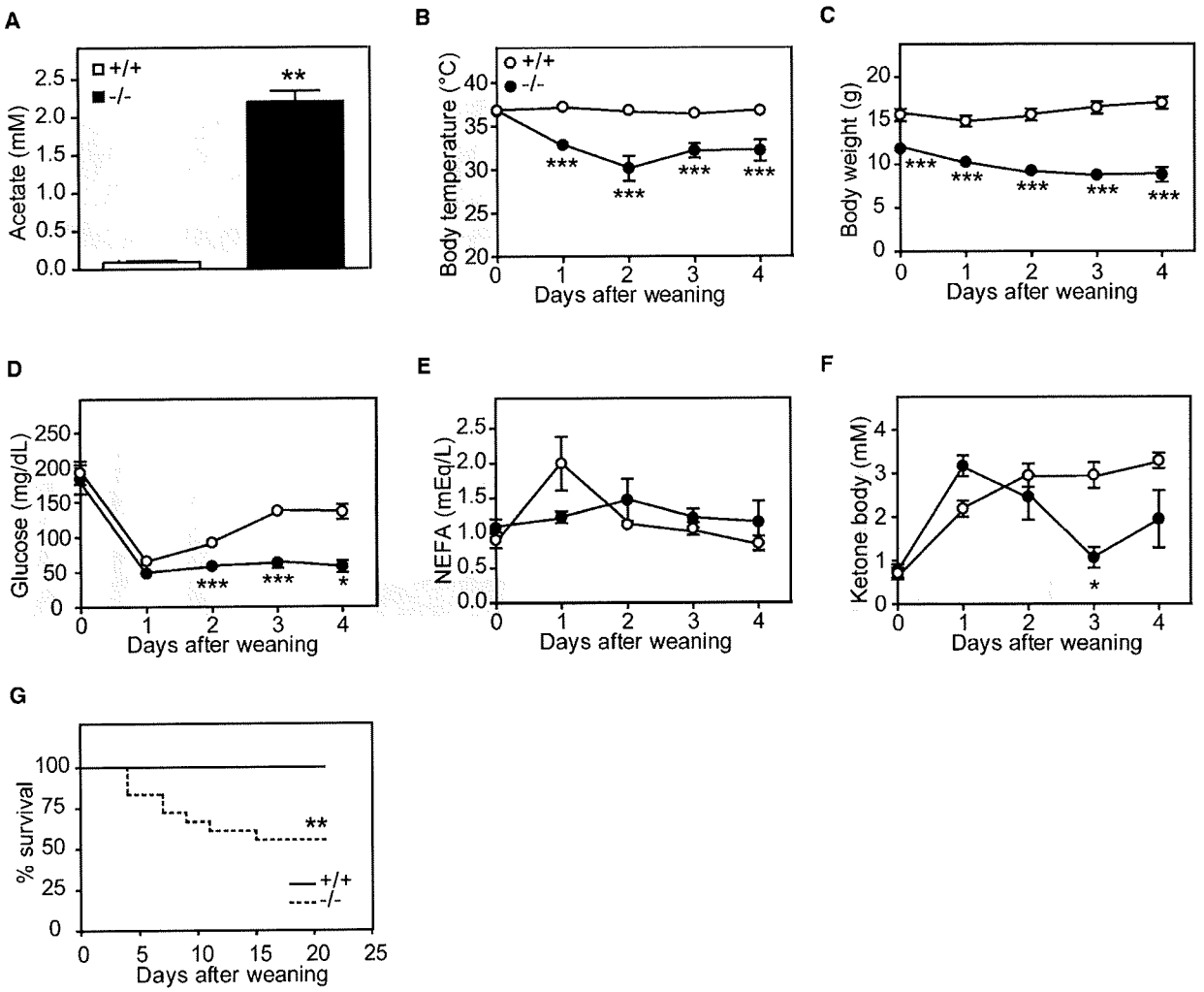


Figure 4. *AceCS2*-Deficient Mice Exhibit Hypothermia When Fed an LC/HF Diet

(A) Male mice (4 weeks old, five per genotype) were fed milk from their mother. Plasma acetate levels were measured.

(B–F) Male mice (4 weeks old) were fed an LC/HF diet. (B) Core rectal temperature, (C) body weight, (D) blood glucose, (E) plasma NEFA, and (F) plasma ketone body level were measured (*AceCS2*$^{+/+}$, n = 8; *AceCS2*$^{-/-}$, n = 7). *p < 0.05, **p < 0.01, and ***p < 0.001 compared to *AceCS2*$^{+/+}$.

(G) Kaplan-Meier analysis of survival in males fed an LC/HF diet at 4 weeks old (*AceCS2*$^{+/+}$, n = 22; *AceCS2*$^{-/-}$, n = 18). **p < 0.001 compared to *AceCS2*$^{+/+}$ by Log-rank test. Data are mean ± SEM.

*AceCS2*$^{+/+}$ and *AceCS2*$^{-/-}$ mice (Figure 5B). We excised various tissues from these mice and measured tissue weights. The photo shown in Figure 5C was taken for representative mice of each group. There were no marked differences in the weights of liver, kidney, BAT, and heart between *AceCS2*$^{+/+}$ and *AceCS2*$^{-/-}$ mice, but the fat pads of *AceCS2*$^{-/-}$ mice were significantly smaller than those of *AceCS2*$^{+/+}$ mice (Figure 5D). We measured metabolic parameters of these mice at 24 weeks of age (Table 2). Although the plasma glucose levels were unchanged, plasma insulin levels decreased significantly in *AceCS2*$^{-/-}$ mice as compared to *AceCS2*$^{+/+}$ mice. Plasma levels of leptin were 4-fold lower, but plasma acetate was 7-fold higher in *AceCS2*$^{-/-}$ mice (Table 2).

In order to investigate the mechanism underlying reduced weight gain in *AceCS2*$^{-/-}$ mice, food intake and energy expenditure were examined. *AceCS2*$^{-/-}$ mice exhibited consistently higher rates of oxygen consumption and, therefore, had higher metabolic rates than *AceCS2*$^{+/+}$ mice throughout day and night (Figure 5E). After adjusting for allometric scaling and gender, the effect of the *AceCS2*$^{-/-}$ allele was highly significant ($p < 0.01$, n = 7, multiple ANOVA) (Figure 5E, right panel). The respiratory quotient was 0.71 in both *AceCS2*$^{+/+}$ and *AceCS2*$^{-/-}$ mice (data not shown). These data suggested that the resistance to weight gain of *AceCS2*$^{-/-}$ mice may be, at least in part, due to increased energy expenditure. To examine the possibility that fatty acids synthesis is changed in *AceCS2*$^{-/-}$ mice, we measured malonyl-CoA levels and acetyl-CoA carboxylase (ACC) activity (Figure S5). Malonyl-CoA levels and ACC activity in skeletal muscle and BAT did not significantly differ between *AceCS2*$^{-/-}$ and *AceCS2*$^{+/+}$ mice (Figure S5). In liver, malonyl-CoA levels

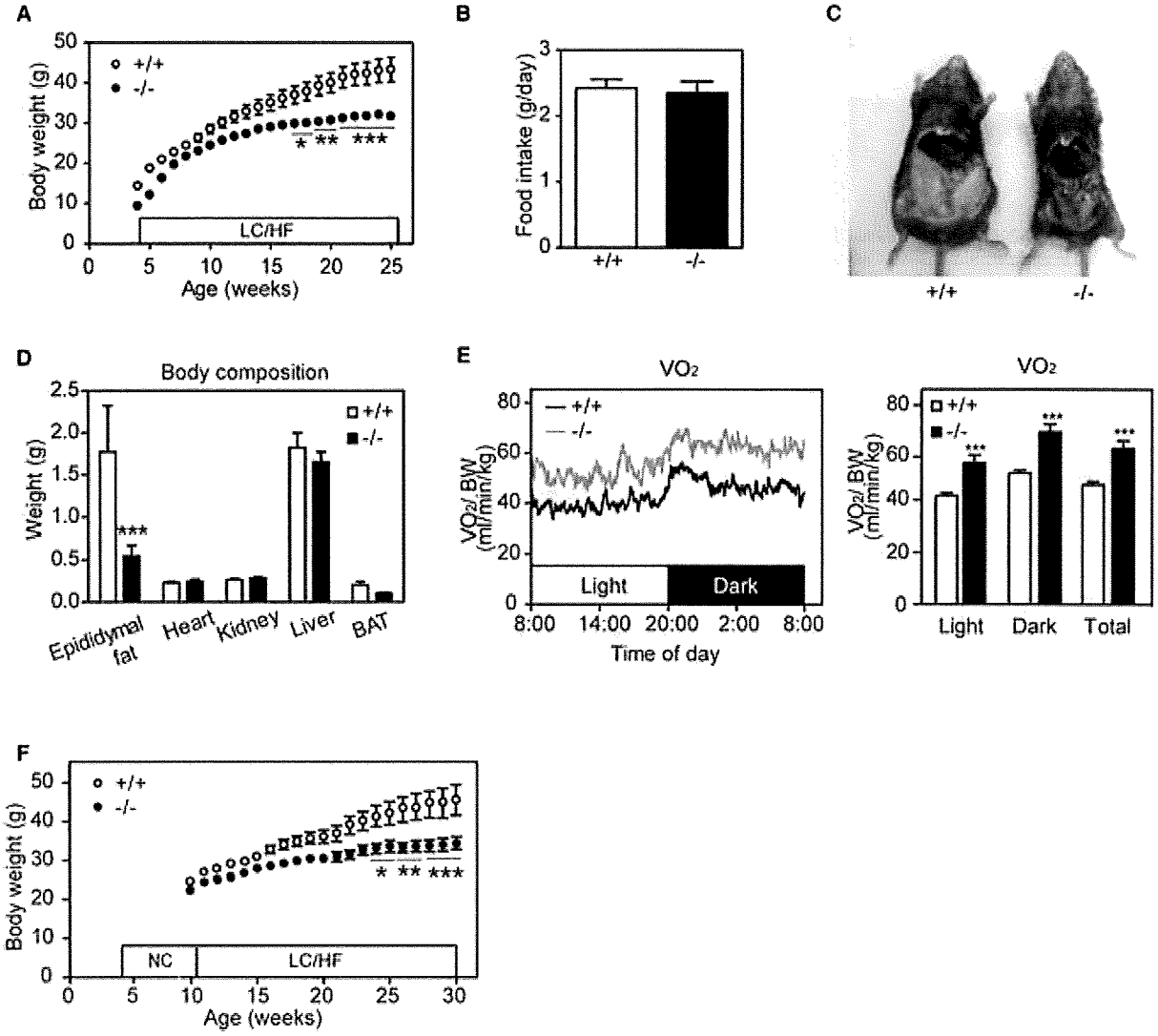


Figure 5. *AceCS2* Deficiency Attenuates Body Weight Gain in Mice Fed an LC/HF Diet

(A) Body weight change of male mice fed an LC/HF diet from 4 weeks old (*AceCS2*$^{+/+}$, n = 15; *AceCS2*$^{-/-}$, n = 12).

(B) Food intake of male mice fed an LC/HF diet at 25 weeks old (*AceCS2*$^{+/+}$, n = 15; *AceCS2*$^{-/-}$, n = 12).

(C) Representative picture of *AceCS2*$^{+/+}$ and *AceCS2*$^{-/-}$ male mice (26 weeks of age) fed an LC/HF diet.

(D) Various tissue weights for *AceCS2*$^{+/+}$ and *AceCS2*$^{-/-}$ male mice (26 weeks of age) fed an LC/HF diet (*AceCS* $^{+/+}$, n = 5; *AceCS2*$^{-/-}$, n = 5).

(E) Oxygen consumption ($VO_2$, left panel) and average of $VO_2$ (right panel) were determined in male mice (26 weeks old) fed an LC/HF diet by indirect calorimetry (*AceCS2*$^{+/+}$, n = 8; *AceCS2*$^{-/-}$, n = 7). Data are corrected for body weight. The original, uncorrected data are shown in Figure S6.

(F) Change of body weight. Male mice were weaned at 4 weeks and were fed on normal chow diet for 6 weeks (until 10 weeks of age) and switched to an LC/HF diet (*AceCS2*$^{+/+}$, n = 8; *AceCS2*$^{-/-}$, n = 8). *$p < 0.05$, **$p < 0.01$, and ***$p < 0.001$ compared to *AceCS2*$^{+/+}$. Data are mean ± SEM. NC, normal chow diet.

were reduced by 20% in *AceCS2*$^{-/-}$ (Figure S5), which could be the secondary effect of lower plasma insulin levels since AceCS2 is not expressed in liver. These data suggested that fatty acid synthesis and degradation are not impaired by the deficiency of *AceCS2*.

It is possible that the reduced weight gain of *AceCS2*$^{-/-}$ mice during LC/HF diet feeding simply resulted from a failure to thrive phenotype (reduced body weight gain, hypothermia, hypoglycemia, and low survival rate) induced by low-carbohydrate diet feeding immediately after weaning (Figure 4). Therefore, after weaning, we first fed the mice a normal chow diet for 6 weeks (until 10 weeks of age) and then switched them to an LC/HF diet. By contrast to feeding an LC/HF diet immediately after weaning, none of these *AceCS2*$^{-/-}$ mice died; however, they did exhibit reduced weight gain compared to *AceCS2*$^{+/+}$ mice following the switch to an LC/HF diet (Figure 5F). Reduced weight gain was observed only under a low-carbohydrate regimen. When mice were fed a high-fat, high-carbohydrate diet, *AceCS2*$^{-/-}$ mice were not protected against weight gain (data not shown). These results clearly indicate that adult

Table 2. Metabolic Parameters of *AceCS2*$^{-/-}$ and *AceCS2*$^{+/+}$ Mice Fed an LC/HF Diet

| | +/+ | −/− |
|---|---|---|
| Glucose (mg/dl) | 233 ± 14 | 233 ± 22 |
| Cholesterol (mg/dl) | 110 ± 7 | 70 ± 11[b] |
| Triglycerides (mg/dl) | 93 ± 6 | 92 ± 9 |
| NEFA (μEql/l) | 343 ± 17 | 332 ± 71 |
| Ketone body (mM) | 0.387 ± 0.064 | 0.705 ± 0.116[a] |
| Leptin (ng/ml) | 2.80 ± 1.12 | 0.74 ± 1.03[b] |
| Insulin (ng/ml) | 3.34 ± 1.3 | 1.54 ± 0.71[a] |
| Acetate (mM) | 0.18 ± 0.06 | 0.97 ± 0.17[b] |

Male mice (24 weeks old, seven to nine per genotype) were fed an LC/HF diet. Assays of blood samples were performed on isolated plasma.
[a] $p < 0.05$.
[b] $p < 0.01$ compared to *AceCS2*$^{+/+}$.

*AceCS2*$^{-/-}$ mice exhibit reduced adiposity under high-fat feeding, low-carbohydrate intake, or ketogenic conditions.

## DISCUSSION

Under ketogenic conditions, free fatty acids are released into the circulation and taken up by thermogenic tissues such as BAT and skeletal muscle, where they serve as a fuel for thermogenesis (Picard et al., 2002; Spiegelman and Flier, 2001). Fatty acids are also taken up by liver for the generation of ketone bodies, and these ketone bodies are subsequently utilized in extrahepatic tissues. In addition, previous studies showed that an appreciable amount of acetate is generated in liver and this acetate can subsequently be utilized by extrahepatic tissues (Leighton et al., 1989; Murthy and Steiner, 1973; Seufert et al., 1974). Here, we demonstrate that acetate also serves as a fuel that has specific functions that do not overlap with those of fatty acids and ketone bodies in thermogenesis.

Our studies of mice with targeted deletion of *AceCS2* reveal that these animals can not maintain normal body temperature when starved or when fed an LC/HF diet. Under these conditions, *AceCS2*$^{-/-}$ mice display sustained hypoglycemia, strongly diminished capacity for exercise, and dramatically increased mortality as compared to their wild-type or heterozygous littermates. The mutant animals also exhibit strikingly reduced rates of whole-body acetate oxidation and correspondingly increased levels of acetate in plasma. Most importantly, ATP levels in the skeletal muscle of 48 hr fasted *AceCS2*$^{-/-}$ mice were profoundly reduced, showing the significant contribution of acetate and AceCS2 to the energy supply under ketogenic conditions. Therefore, under ketogenic conditions, the hypothermia and poor exercise tolerance observed in the *AceCS2*$^{-/-}$ mice is most likely from a lack of acetate utilization as a fuel source. Supporting this possibility, plasma acetate levels were significantly higher under fasting conditions than under fed conditions. This suggests that acetate turnover is significantly higher in the fasted state primarily due to AceCS2.

LC/HF diet has been generally recognized to have weight-reducing effects on obese animals (Kennedy et al., 2007). Although the body weight gain of mice fed an LC/HF diet is significantly lower than that of those fed high-fat and high-carbohydrate diets, our LC/HF diet has no weight-reducing or anti-weight-gaining effect. In the experiments done by Kennedy et al. (2007), 8-week-old mice fed a normal chow diet were switched to an LC/HF diet, and the weight of mice fed an LC/HF diet dropped until it stabilized at 85% of the initial weight. The discrepancy between these results may result from the difference in the composition of the different LC/HF diets. The LC/HF diet that Kennedy et al. used consists of 78.85% fat, 9.5% protein, and 0.76% carbohydrate, whereas our LC/HF diet (purchased from Harlan Teklad) contains 67.4% fat, 15.3% protein, and 0.6% carbohydrate (% by weight). In addition, the source of the fat is also different. The LC/HF diet in their study contains lard and butter, whereas our LC/HF diet contains vegetable shortening. Regardless of the differences in the exact diet, we show that AceCS2 is critical for normal body weight gain under an LC/HF diet.

Recent observations indirectly support a role for *AceCS2* as a determinant of growth and adiposity. From the mapping of a quantitative trait locus (QTL) region on mouse chromosome 2 that has a large effect on growth and adiposity, AceCS2 was reported as 1 of 18 candidate genes potentially controlling predisposition to growth and predisposition to obesity (Jerez-Timaure et al., 2005).

Although plasma acetate is very high in *AceCS2*$^{-/-}$ mice, we found that there was appropriate and sufficient respiratory compensation for any metabolic acidosis caused by acetate accumulation. *AceCS2*$^{-/-}$ mice exhibited hypocapnea to maintain a neutral arterial blood pH. Patients with chronic obstructive lung disease and cystic fibrosis commonly have low body weight, which is believed to be related to inadequate energy intake, nutrient malabsorption, and excessive energy expenditure (Bell et al., 1996). Basal metabolic rate is 10%–20% greater in these patients than in healthy subjects and may contribute to their energy imbalance. Furthermore, increased oxygen consumption caused by increased respiratory muscle activity has been reported in these patients, which largely explains the increased basal metabolic rate (Campbell et al., 1959; Cherniack, 1959; Donahoe et al., 1989; McGregor and Becklake, 1961). Because *AceCS2*$^{-/-}$ mice seem to be hyperventilating, this increased use of respiratory muscles might account for, at least in part, the higher oxygen consumption.

We previously identified AceCS2 as a target of KLF15 (Yamamoto et al., 2004). The fasting-induced transcription of AceCS2 is largely dependent on KLF15. Similarly to *AceCS2*$^{-/-}$ mice, KLF15-deficient mice also exhibit severe hypoglycemia after overnight fasting (Fisch et al., 2007). KLF15 plays an important role in gluconeogenesis by regulating amino acid degradation and key gluconeogenic enzymes such as phosphoenolpyruvate carboxykinase in the liver during fasting (Gray et al., 2007; Teshigawara et al., 2005). Our data indicate that KLF15 is crucial for survival during starvation through two mechanisms: (1) gluconeogenesis in liver and (2) acetate oxidation to generate ATP and heat in muscle and BAT through AceCS2 activity.

The sirtuins comprise a conserved family of proteins that are believed to mediate some of the health benefits of calorie restriction, which leads to extension of life span in nearly all organisms studied, including mammals. SIRT1 has been reported to function as an energy-sensing gene that senses $NAD^+$ levels and regulates the activity of critical transcriptional regulators of

metabolism in multiple tissues (Yang et al., 2007). Within the mitochondria, SIRT3 deacetylates a key lysine residue on AceCS2, leading to its enzymatic activation (Hallows et al., 2006; Schwer et al., 2006; Schwer and Verdin, 2008). As SIRT3 protein levels are specifically increased in calorie-restricted mammals, regulation of AceCS2 activity by SIRT3 could be a key metabolic factor responsible for homeostatic regulation during calorie restriction, leading to its positive effect on life span. Sirt3 was recently shown to be necessary for maintaining basal ATP levels with ATP levels in multiple organs of *Sirt3*$^{-/-}$ mice that are markedly reduced compared to wild-type levels (Ahn et al., 2008). This study, along with ours, suggests that activation of AceCS2 by Sirt3 is required to maintain basal ATP levels in mammals. Future studies of AceCS2- and AceCS2-deficient mice are warranted to investigate this potentially exciting link between longevity and mitochondrial energy metabolism.

In conclusion, our current findings demonstrate that acetate metabolism mediated by AceCS2 is crucial for survival and energy production under ketogenic conditions such as starvation or diabetes. These and future studies of acetate metabolism mediated by AceCS2 will have a significant impact on the understanding of the acetate metabolism for heat generation and energy metabolism.

## EXPERIMENTAL PROCEDURES

### Generation of AceCS2-Deficient Mice

We constructed a targeting plasmid by using genomic DNA fragments derived from Sv129 mice. A Lac Z and a neomycin cassette flanked by two loxP sites were introduced into the *AceCS2* locus of ES cells (derived from the Sv129 strain). Electroporation, selection, and screening were performed with standard gene-targeting techniques. Briefly, genomic DNA was isolated from neomycin-resistant ES cell clones, digested with KpnI, and subjected to hybridization with a probe to detect homologous recombination and the presence of the flox allele (Figure 1A).

Chimeric males were generated by using the morula aggregation technique and mated to C57BL/6J female mice. Homologous recombination was confirmed by Southern blotting (Figure 1B). Deletion of RNA transcripts and protein was confirmed by QRT-PCR and western blotting, respectively (Figures 1D and 1E). After achieving germline transmission, *AceCS2*$^{+/-}$ mice were crossed with C57BL/6J for six to nine generations.

Heterozygous mice were mated to obtain *AceCS2*$^{-/-}$ mice. Wild-type littermates were used as controls throughout the study. Genotyping of mice used in this study was performed by PCR of tail DNA as shown in Figure 1C; the mutant allele was detected by using a pair of oligonucleotides (5′-GGCGCACAA CAAAACCTAGT-3′ and 5′-GACAGTATCGGCCTCAGGAA-3′) that amplify a 512 bp PCR product between the *AceCS2* and sequence 3′ to *Lac Z/neo* cassette. The wild-type allele was detected by PCR with a pair of oligonucleotides (5′-GGCGCACAACAAAACCTAGT-3′ and 5′-GGGGTTCGTGCCTGGTTG-3′) that amplify a 355 bp PCR product spanning exon 1.

### Quantitative Real-Time PCR

Quantitative real-time PCR (QRT-PCR) was performed as previously described (Tanaka et al., 2003). All primer sequences used in this paper are available upon request.

### Antibody

To produce rabbit polyclonal anti-murine AceCS2 (IgGA001), a 12-residue peptide corresponding to the C terminus of murine AceCS2 (CQKYEEQ RAATN) was synthesized (Sigma Genesis, Japan), coupled to keyhole limpet hemocyanin, and injected into New Zealand White rabbits. IgG fractions were prepared by affinity chromatography on protein A-Sepharose (GE Healthcare Bioscience). For immunoblot analysis, an aliquot of whole-cell lysates from heart (20 μg) was subjected to SDS-PAGE on 10% gels followed by analysis with a 1:1000 dilution of anti-AceCS2 (Fujino et al., 2001).

### Animal Experiments

All procedures were performed in accordance with Japanese Physiological Society guidelines for animal care. Mice were group housed in cages with a 12 hr light/12 hr dark cycle and fed a standard rodent chow diet (CE-2; CLEA Japan, Osaka). To induce a ketogenic condition, we compared an LC/HF diet (Table S3; Rho et al., 1999) (TD96355; Harlan Teklad Premier Laboratory Diets) consisting of 90.5% fat, 9.1% protein, and 0.4% carbohydrate (0% sucrose from calories) to a high-carbohydrate, high-fat diet consisting of 58.0% fat, 15.0% protein, and 27.01% carbohydrate from calories (Tanaka et al., 2003). All mice had free access to water. Food consumption was monitored daily, and body weight was recorded every week, unless otherwise stated.

Core body temperature was monitored using a rectal thermometer at 10 a.m. For the exercise performance, the mice were trained on the treadmill (MK-680AT/02M, Muromachikikai, Tokyo) prior to the exercise performance test (a 10 min run at 10 m/min at a 5° incline once per day for 4 days). Exhaustion was defined as the point at which mice were unable to continue running.

### Food Intake, Locomotor Activity, and Metabolic Rate Measurement

Male mice (26 weeks old) were housed under controlled lighting (12 hr light-dark cycle) and temperature (23°C) conditions. Food (standard chow pellets or an LC/HF diet) and water were available ad libitum. Mice were then housed singly under the same conditions as above for an acclimation period of at least 7 days. Body weights and food intake were monitored daily for the duration of the study. Energy expenditure was measured by indirect calorimetry as described previously (MK-5000RQ; Muromachi, Tokyo) (Takayasu et al., 2006). Mice were placed in the calorimeter chambers and acclimated for 1 day. Locomotor activity was measured by using an infrared (IR) passive sensor system as described previously (Supermex, Muromachi Kikai, Japan) (Takayasu et al., 2006). The experiment was started at 8 a.m. (light period).

### Acetate Oxidation

Acetate ([1-$^{14}$C]acetate, CFA13, GE Healthcare UK Limited) oxidation was measured in vivo as described (Wolfgang et al., 2006). The in vivo rate of $^{14}$C-acetate oxidation (2 μCi [1 Ci = 37 GBq] of [1-$^{14}$C]acetate injected intraperitoneally) to $^{14}CO_2$ was determined after treatment of mice. Mice were acclimated in metabolic chambers fitted with 2-aminoethanol traps to recover expired $^{14}CO_2$. The oxidation of [1-$^{14}$C]acetate to form $^{14}CO_2$ was measured at 20 min intervals over the next 1 hr. At the end of experiment, plasma was collected, and plasma [1-$^{14}$C]acetate was measured.

### Acetate Measurement

Plasma acetate levels were measured as described by (Hillman et al. 1978) with slight modifications. Briefly, plasma was mixed with 1 mM isovaleric acid as the internal standard. The sample was acidified with one-fifth the volume of 10% sulfosalicylic acid and then extracted three times with 10 volumes of diethylether. The ether extract was immediately back extracted into 0.2 M NaOH. The ether was removed under a stream of dry nitrogen. Before injection, the sample was reacidified with one-fifth the volume of 10% phosphoric acid. The acetate concentration of the sample was analyzed by gas chromatograph (GC-2014, Shimadzu, Japan) equipped with a flame ionization detector and a capillary column (ULBON HR-20 M, 0.25 mm i.d. × 25 m × 0.25 μm). The column was operated at 140°C. The injection port and the flame ionization detector were maintained at 300°C. The chromatograph was standardized with a mixture of C2-C7 short-chain fatty acids.

### Plasma Parameters

Mice were sacrificed by $CO_2$ asphyxiation following a 4 hr fast during the light cycle (food removed 9:00 a.m., sacrificed at 1:00 p.m.). Blood was drawn by cardiac puncture, and the plasma was separated immediately by centrifugation and stored at −80°C until use. Plasma glucose, NEFA, triglycerides, total cholesterol, and total ketone body levels were determined by Glucose C2-test (Wako Pure Chemical, Japan), NEFA C-test (Wako Pure Chemical, Japan), Triglyceride E-test (Wako Pure Chemical, Japan), Cholesterol E-test (Wako Pure Chemical, Japan), and Autokit Total Ketone Bodies (Wako Pure

Chemical, Japan), respectively. Plasma insulin and leptin levels were determined by ELISA with an insulin immunoassay kit (Shibayagi, Japan) and a mouse leptin immunoassay (R & D systems) according to the manufacturer's instructions.

### Assay Procedure for Acetyl-CoA, Adenine Nucleotides, $NAD^+$, and NADH Contents

Acetyl-CoA and adenine nucleotide contents in skeletal muscle or BAT of 12-week-old male mice were measured essentially as described previously (Miura et al., 2006; Scott et al., 1992; Takamura et al., 1985). $NAD^+$ and NADH nucleotide concentrations were directly measured by $NAD^+$/NADH Assay kit (Biochain Institute, Inc.) according to the manufacturer's instructions. The detail methods are described in the Supplemental Experimental Procedures.

### Blood Gas Analysis

Blood gas analysis was performed as previously described (Kuwaki et al., 1996). A catheter was implanted into the right femoral artery under isoflurane (2%–3%) anesthesia. Up to 70 μl of arterial blood was drawn from the indwelling catheter after a recovery period of more than 2 hr and when the animal was quietly awake. Blood gases were determined by a blood gas analyzer (ABL500, Radiometer, Copenhagen).

### Statistical Analyses

All values are expressed as mean ± standard error of the mean unless otherwise specified. Significant differences between mean values were evaluated using two-tailed, unpaired Student's t test (when two groups were analyzed) or one-way ANOVA followed by Student Newman-Keuls test (for three or more groups).

## SUPPLEMENTAL DATA

Supplemental Data include Supplemental Experimental Procedures, six figures, and three tables and can be found with this article online at: http://www.cell.com/cell-metabolism/supplemental/S1550-4131(08)00393-8.

## ACKNOWLEDGMENTS

We thank Dr. Rob Rawson for critical reading of the manuscript; Drs. Peter Edwards and Mitsuhiro Watanabe for helpful discussions; and Kaori Ikeda, Junko Kuno, Satomi Takahashi, Yuko Kai, and Mika Nomiyama for technical assistance. This work was supported through ERATO JST, NIBIO by the NFAT project of the NEDO and by the Special Coordination Fund for Science and Technology from the Ministry of Education, Culture, Sports, Science, and Technology. This work was also supported, in part, by Astellas Foundation for Research on Metabolic Disorders, the Uehara Memorial Foundation, and the Ono Medical Foundation. M.Y. is an Investigator of the Howard Hughes Medical Institute. J.S. is an Investigator of Translational Systems Biology and Medicine Initiative (TSBMI).

Received: June 6, 2008
Revised: October 15, 2008
Accepted: December 12, 2008
Published: February 3, 2009

## REFERENCES

Ahn, B.H., Kim, H.S., Song, S., Lee, I.H., Liu, J., Vassilopoulos, A., Deng, C.X., and Finkel, T. (2008). A role for the mitochondrial deacetylase Sirt3 in regulating energy homeostasis. Proc. Natl. Acad. Sci. USA *105*, 14447–14452.

Bell, S.C., Saunders, M.J., Elborn, J.S., and Shale, D.J. (1996). Resting energy expenditure and oxygen cost of breathing in patients with cystic fibrosis. Thorax *51*, 126–131.

Campbell, E.J., Westlake, E.K., and Cherniack, R.M. (1959). The oxygen consumption and efficiency of the respiratory muscles of young male subjects. Clin. Sci. (Lond.) *18*, 55–64.

Cherniack, R.M. (1959). The oxygen consumption and efficiency of the respiratory muscles in health and emphysema. J. Clin. Invest. *38*, 494–499.

Donahoe, M., Rogers, R.M., Wilson, D.O., and Pennock, B.E. (1989). Oxygen consumption of the respiratory muscles in normal and in malnourished patients with chronic obstructive pulmonary disease. Am. Rev. Respir. Dis. *140*, 385–391.

Fisch, S., Gray, S., Heymans, S., Haldar, S.M., Wang, B., Pfister, O., Cui, L., Kumar, A., Lin, Z., Sen-Banerjee, S., et al. (2007). Kruppel-like factor 15 is a regulator of cardiomyocyte hypertrophy. Proc. Natl. Acad. Sci. USA *104*, 7074–7079.

Fujino, T., Kondo, J., Ishikawa, M., Morikawa, K., and Yamamoto, T.T. (2001). Acetyl-CoA synthetase 2, a mitochondrial matrix enzyme involved in the oxidation of acetate. J. Biol. Chem. *276*, 11420–11426.

Fukao, T., Lopaschuk, G.D., and Mitchell, G.A. (2004). Pathways and control of ketone body metabolism: On the fringe of lipid biochemistry. Prostaglandins Leukot. Essent. Fatty Acids *70*, 243–251.

Gray, S., Wang, B., Orihuela, Y., Hong, E.G., Fisch, S., Haldar, S., Cline, G.W., Kim, J.K., Peroni, O.D., Kahn, B.B., et al. (2007). Regulation of gluconeogenesis by Kruppel-like factor 15. Cell Metab. *5*, 305–312.

Hallows, W.C., Lee, S., and Denu, J.M. (2006). Sirtuins deacetylate and activate mammalian acetyl-CoA synthetases. Proc. Natl. Acad. Sci. USA *103*, 10230–10235.

Hillman, R.E. (1978). Simple, rapid method for determination of propionic acid and other short-chain fatty acids in serum. Clin. Chem. *24*, 800–803.

Ikeda, Y., Yamamoto, J., Okamura, M., Fujino, T., Takahashi, S., Takeuchi, K., Osborne, T.F., Yamamoto, T.T., Ito, S., and Sakai, J. (2001). Transcriptional regulation of the murine acetyl-CoA synthetase 1 gene through multiple clustered binding sites for sterol regulatory element-binding proteins and a single neighboring site for Sp1. J. Biol. Chem. *276*, 34259–34269.

Jerez-Timaure, N.C., Eisen, E.J., and Pomp, D. (2005). Fine mapping of a QTL region with large effects on growth and fatness on mouse chromosome 2. Physiol. Genomics *21*, 411–422.

Kennedy, A.R., Pissios, P., Otu, H., Xue, B., Asakura, K., Furukawa, N., Marino, F.E., Liu, F.F., Kahn, B.B., Libermann, T.A., et al. (2007). A high-fat, ketogenic diet induces a unique metabolic state in mice. Am. J. Physiol. Endocrinol. Metab. *292*, E1724–E1739.

Kuwaki, T., Cao, W.H., Kurihara, Y., Kurihara, H., Ling, G.Y., Onodera, M., Ju, K.H., Yazaki, Y., and Kumada, M. (1996). Impaired ventilatory responses to hypoxia and hypercapnia in mutant mice deficient in endothelin-1. Am. J. Physiol. *270*, R1279–R1286.

Leighton, F., Bergseth, S., Rortveit, T., Christiansen, E.N., and Bremer, J. (1989). Free acetate production by rat hepatocytes during peroxisomal fatty acid and dicarboxylic acid oxidation. J. Biol. Chem. *264*, 10347–10350.

Lowell, B.B., and Spiegelman, B.M. (2000). Towards a molecular understanding of adaptive thermogenesis. Nature *404*, 652–660.

Luong, A., Hannah, V.C., Brown, M.S., and Goldstein, J.L. (2000). Molecular characterization of human acetyl-CoA synthetase, an enzyme regulated by sterol regulatory element-binding proteins. J. Biol. Chem. *275*, 26458–26466.

Matthias, A., Ohlson, K.B., Fredriksson, J.M., Jacobsson, A., Nedergaard, J., and Cannon, B. (2000). Thermogenic responses in brown fat cells are fully UCP1-dependent. UCP2 or UCP3 do not substitute for UCP1 in adrenergically or fatty scid-induced thermogenesis. J. Biol. Chem. *275*, 25073–25081.

McGregor, M., and Becklake, M.R. (1961). The relationship of oxygen cost of breathing to respiratory mechanical work and respiratory force. J. Clin. Invest. *40*, 971–980.

Miura, S., Tomitsuka, E., Kamei, Y., Yamazaki, T., Kai, Y., Tamura, M., Kita, K., Nishino, I., and Ezaki, O. (2006). Overexpression of peroxisome proliferator-activated receptor gamma co-activator-1alpha leads to muscle atrophy with depletion of ATP. Am. J. Pathol. *169*, 1129–1139.

Murthy, V.K., and Steiner, G. (1973). Hepatic acetate levels in relation to altered lipid metabolism. Metabolism *22*, 81–84.

Picard, F., Gehin, M., Annicotte, J., Rocchi, S., Champy, M.F., O'Malley, B.W., Chambon, P., and Auwerx, J. (2002). SRC-1 and TIF2 control energy balance between white and brown adipose tissues. Cell *111*, 931–941.

Rho, J.M., Kim, D.W., Robbins, C.A., Anderson, G.D., and Schwartzkroin, P.A. (1999). Age-dependent differences in flurothyl seizure sensitivity in mice treated with a ketogenic diet. Epilepsy Res. *37*, 233–240.

Schwer, B., Bunkenborg, J., Verdin, R.O., Andersen, J.S., and Verdin, E. (2006). Reversible lysine acetylation controls the activity of the mitochondrial enzyme acetyl-CoA synthetase 2. Proc. Natl. Acad. Sci. USA *103*, 10224–10229.

Schwer, B., and Verdin, E. (2008). Conserved metabolic regulatory functions of sirtuins. Cell Metab. *7*, 104–112.

Scott, M.D., Baudendistel, L.J., and Dahms, T.E. (1992). Rapid separation of creatine, phosphocreatine and adenosine metabolites by ion-pair reversed-phase high-performance liquid chromatography in plasma and cardiac tissue. J. Chromatogr. *576*, 149–154.

Seufert, C.D., Graf, M., Janson, G., Kuhn, A., and Soling, H.D. (1974). Formation of free acetate by isolated perfused livers from normal, starved and diabetic rats. Biochem. Biophys. Res. Commun. *57*, 901–909.

Spiegelman, B.M., and Flier, J.S. (2001). Obesity and the regulation of energy balance. Cell *104*, 531–543.

Takamura, Y., Kitayama, Y., Arakawa, A., Yamanaka, S., Tosaki, M., and Ogawa, Y. (1985). Malonyl-CoA: Acetyl-CoA cycling. A new micromethod for determination of acyl-CoAs with malonate decarboxylase. Biochim. Biophys. Acta *834*, 1–7.

Takayasu, S., Sakurai, T., Iwasaki, S., Teranishi, H., Yamanaka, A., Williams, S.C., Iguchi, H., Kawasawa, Y.I., Ikeda, Y., Sakakibara, I., et al. (2006). A neuropeptide ligand of the G protein-coupled receptor GPR103 regulates feeding, behavioral arousal, and blood pressure in mice. Proc. Natl. Acad. Sci. USA *103*, 7438–7443.

Tanaka, T., Yamamoto, J., Iwasaki, S., Asaba, H., Hamura, H., Ikeda, Y., Watanabe, M., Magoori, K., Ioka, R.X., Tachibana, K., et al. (2003). Activation of peroxisome proliferator-activated receptor delta induces fatty acid beta-oxidation in skeletal muscle and attenuates metabolic syndrome. Proc. Natl. Acad. Sci. USA *100*, 15924–15929.

Teshigawara, K., Ogawa, W., Mori, T., Matsuki, Y., Watanabe, E., Hiramatsu, R., Inoue, H., Miyake, K., Sakaue, H., and Kasuga, M. (2005). Role of Kruppel-like factor 15 in PEPCK gene expression in the liver. Biochem. Biophys. Res. Commun. *327*, 920–926.

Wolfgang, M.J., Kurama, T., Dai, Y., Suwa, A., Asaumi, M., Matsumoto, S., Cha, S.H., Shimokawa, T., and Lane, M.D. (2006). The brain-specific carnitine palmitoyltransferase-1c regulates energy homeostasis. Proc. Natl. Acad. Sci. USA *103*, 7282–7287.

Yamamoto, J., Ikeda, Y., Iguchi, H., Fujino, T., Tanaka, T., Asaba, H., Iwasaki, S., Ioka, R.X., Kaneko, I.W., Magoori, K., et al. (2004). A Kruppel-like factor KLF15 contributes fasting-induced transcriptional activation of mitochondrial acetyl-CoA synthetase gene AceCS2. J. Biol. Chem. *279*, 16954–16962.

Yamashita, H., Kaneyuki, T., and Tagawa, K. (2001). Production of acetate in the liver and its utilization in peripheral tissues. Biochim. Biophys. Acta *1532*, 79–87.

Yang, H., Yang, T., Baur, J.A., Perez, E., Matsui, T., Carmona, J.J., Lamming, D.W., Souza-Pinto, N.C., Bohr, V.A., Rosenzweig, A., et al. (2007). Nutrient-sensitive mitochondrial NAD+ levels dictate cell survival. Cell *130*, 1095–1107.

Mitochondrion 9 (2009) 443–453

Contents lists available at ScienceDirect

Mitochondrion

journal homepage: www.elsevier.com/locate/mito

# Identification of mitochondrial Complex II subunits SDH3 and SDH4 and ATP synthase subunits *a* and *b* in *Plasmodium* spp.

Tatsushi Mogi *, Kiyoshi Kita *

*Department of Biomedical Chemistry, Graduate School of Medicine, The University of Tokyo, Hongo, Bunkyo-ku, Tokyo 113-0033, Japan*

ARTICLE INFO

*Article history:*
Received 5 February 2009
Received in revised form 3 August 2009
Accepted 6 August 2009
Available online 12 August 2009

*Keywords:*
ATP synthase
Membrane anchor
Mitochondria
*Plasmodium*
Succinate dehydrogenase

ABSTRACT

While most protist mitochondrial enzymes could be identified in database, the membrane anchor subunits of Complex II and $F_oF_1$-ATP synthase of malaria parasites are not annotated. Based on the presence of structural fingerprints or proteomics data from other protists, here we present their candidates. In contrast to canonical subunits, *Plasmodium* Complex II anchors have two transmembrane helices and may coordinate heme *b via* Tyr in place of His. Transmembrane helix IV of ATP synthase subunit *a* lacks an essential Arg residue. Membrane anchors of *Plasmodium* Complex II and ATP synthase are divergent from orthologs and promising targets for new chemotherapeutics.



## 1. Introduction

Energy metabolism in the malaria parasites is quite different from that of mammalian hosts. The erythrocytic stage cells of *Plasmodium falciparum* cause mortality associated with malaria and are considered to rely on the incomplete oxidation of glucose, with the secretion of end products such as lactate and pyruvate (Sherman, 1998). Diversity in parasite metabolism and enzyme structures will facilitate the development of new antimalarials with novel targets and mechanisms against the drug-resistant strains of *Plasmodium* spp. (Hyde, 2005).

The *Plasmodium* mitochondrion of the erythrocytic stage parasites can oxidize NADH, glycerol-3-phosphate, succinate, dihydroorotate, and amino acids (Pro and Glu), but it is essentially acristate and apparently lacks oxidative phosphorylation and a functional tricarboxylic acid (TCA) cycle (Fry and Beesley, 1991; van Dooren et al., 2006). Pyruvate dehydrogenase is targeted to the apicoplast, not to the mitochondrion (Foth et al., 2005), and thus a major carbon flow from the cytoplasm to the mitochondrion of most eukaryotes is disconnected (Fig. 1). Fumarate inhibited the NADH-dependent reduction of cytochrome *c* and stimulated the oxidation of NADH, indicating an NADH–fumarate reductase pathway for the regeneration of NAD (Fry and Beesley, 1991). Recently, Painter et al. (2007) claimed for the erythrocytic stage cells of *P. falciparum* that the mitochondrial respiratory chain is required only for the regeneration of an oxidized form of ubiquinone, which serves as the electron acceptor for type 2 dihydroorotate dehydrogenase, an essential enzyme for pyrimidine biosynthesis. Thus, it is widely accepted that the majority of the erythrocytic stage parasite's ATP demand is met through glycolysis (Carlton et al., 2002).

In the insect vector stages, malaria parasites need to adapt to changes in available carbon sources from glucose in the mammalian blood to amino acids (e.g., Pro, Glu, His, and Ala (Henn et al., 1998)) in the mosquito hemolymph, which contains the disaccharide trehalose as a dominant sugar species. As amino acids are non-fermentable carbon sources, oxidative phosphorylation with the functional TCA cycle must take place in the insect stages. Proteomic profiling studies clearly demonstrated metabolic readjustments from the glycolytic pathway in the asexual stages trophozoites and schizonts to the TCA cycle in the salivary gland sporozoites (Lasonder et al., 2008). Metabolomic studies on the erythrocytic stage *P. falciparum* demonstrated that Gln was metabolized to L-malate *via* two pathways, the reductive carboxylation pathway through citrate yielding acetyl-CoA and the oxidative pathway through succinate yielding ATP and a precursor of heme biosynthesis (δ-aminolevulinic acid) (Olszewski, Rabinowitz, Llinás, personal communication) (Fig. 1). Thus, amino acids acquired from the mosquito hemolymph or the food vacuole of the erythrocytic stage parasites can be metabolized by entering the TCA cycle as 2-oxoglutarate *via* a bifurcated mechanism using

*Abbreviations:* FRD, fumarate reductase; SDH, succinate dehydrogenase; TCA, tricarboxylic acid; TM, transmembrane helix.

* Corresponding authors. Tel.: +81 3 5841 3526; fax: +81 3 5841 3444.
*E-mail addresses:* tmogi@m.u-tokyo.ac.jp (T. Mogi), kitak@m.u-tokyo.ac.jp (K. Kita).

1567-7249/$ - see front matter © 2009 Elsevier B.V. and Mitochondria Research Society. All rights reserved.
doi:10.1016/j.mito.2009.08.004

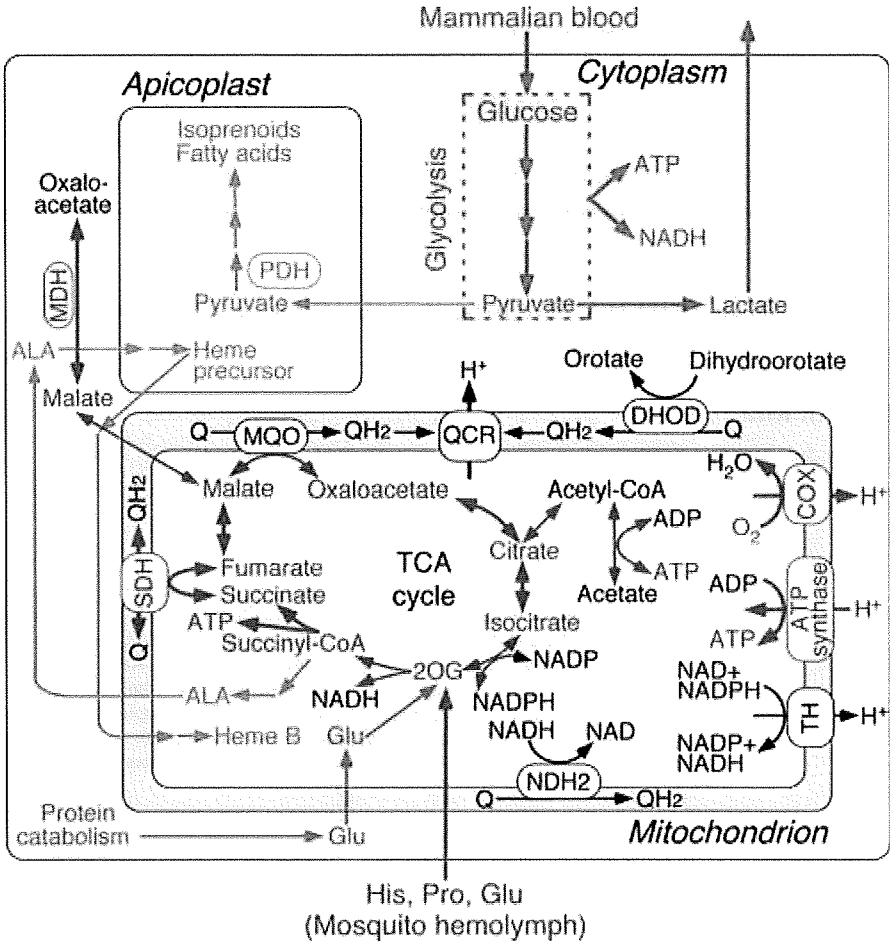


**Fig. 1.** Metabolic pathway in the human malaria parasite *P. falciparum*. Proton translocation machineries in the mitochondrion are $F_oF_1$-ATP synthase (ATPase), quinol–cytochrome *c* reductase (QCR), cytochrome *c* oxidase (COX), and NAD(P)-transhydrogenase (TH). Quinone reduction by alternative NADH dehydrogenase (NDH2), succinate dehydrogenase (SDH), malate:quinone oxidoreductase (MQO), and dihydroorotate dehydrogenase (DHOD) do not generate the proton-motive force. NAD-dependent malate dehydrogenase (MDH) and pyruvate dehydrogenase (PDH) are located in the cytoplasm and apicoplast, respectively, and do not participate in TCA cycle. Expression levels of MDH and TCA cycle enzymes (fumarate hydratase, SDH1, succinyl-CoA synthase α subunit, aconitase, and citrate synthase), and α and β subunits of ATP synthase are increased in salivary gland sporozoites while the expression levels of glycolysis pathway enzymes (hexokinase, phosphoglycerate kinase, pyruvate kinase and 6-phosphofructokinase) are increased in asexual blood-stage trophozoites and schizonts [Lasonder et al., 2008; Lasonder, Stunnenberg, personal communication]. A major carbon flow in blood-stage parasites is shown in *red* and possible carbon and energy flow in mosquito stages is shown in *blue*. Pathways absent in *B. bovis* are indicated by *green*. For the clarity, outer membranes of the mitochondrion and apicoplast are not shown. Abbreviations for metabolites are ALA (δ-aminolevulinic acid), DHAP (dihydroxyacetone phosphate), GA3P (glyceraldehyde-3-phosphate), and PEP (phosphoenolpyruvate).

the reductive and oxidative pathways. The resulting NADH and quinols are reoxidized by the respiratory chain, which indirectly drives ATP synthesis by the generation of proton-motive force.

In contrast to *P. falciparum*, the mitochondrion isolated from the erythrocytic stage rodent malaria parasite is cristate and contains more cytochromes (Fry and Beesley, 1991). Succinate respiration, ATP synthesis, and the collapse of the mitochondrial membrane potential by atovaquone (Srivastava et al., 1997), a potent inhibitor of ubiquinol–cytochrome *c* reductase (Complex III), suggest the presence of a functional oxidative phosphorylation system in the erythrocytic rodent parasite mitochondria (Uyemura et al., 2000, 2004). Transcriptome analysis of the erythrocytic human parasites, which have been isolated from infected patients, indicates that canonical mitochondrial functions exist to some extent in the human parasites (Daily et al., 2007). In *Plasmodium* spp., nuclear and mitochondrial genomes encode ubiquinol–cytochrome *c* reductase (QCR, Complex III), cytochrome *c* oxidase (COX, Complex IV), $F_oF_1$-ATP synthase (Complex V) and all the TCA cycle enzymes including succinate dehydrogenase (SDH, succinate–ubiquinone reductase, Complex II) (Carlton et al., 2002; Gardner et al., 2002). $H^+$-translocating NADH–ubiquinone reductase (NDH1, Complex I) in the mitochondrial respiratory chain is substituted by alternative NADH dehydrogenase (NDH2, a single-subunit NADH–ubiquinone reductase) (Uyemura et al., 2004; Biagini et al., 2006; Kawahara et al., 2009) (Fig. 1).

It should be noted that the membrane anchor subunits of Complex II (SDH3 (CybL) and SDH4 (CybS)) and of ATP synthase (subunits *a* (ATP6) and *b* (ATP4)) are not annotated in the current database (Carlton et al., 2002; Gardner et al., 2002), even though they are essential for transfer of chemical energy to ubiquinone and proton translocation, respectively (Fig. 2). Accordingly, the complete ATP synthase is assumed to be absent in *Plasmodium* spp. (Carlton et al., 2002; Gardner et al., 2002; Fry et al., 1990; Vaidya and Mather, 2005).

Recently, we characterized characterized Complex II of the erythrocytic stage *Plasmodium yoelii yoelii* mitochondria and found evidence for the presence of SDH3 and SDH4 (Kawahara et al., 2009). Because of the low expression of TCA cycle enzymes in

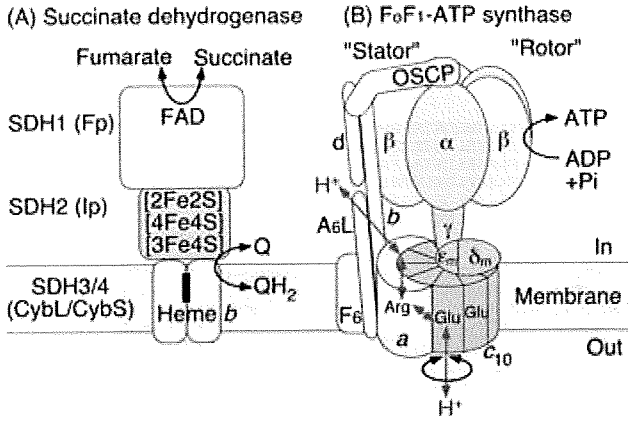


**Fig. 2.** Structure model for protist Complex II and ATP synthase.

the erythrocytic stage cells (Lasonder et al., 2008), sequence analysis of the anchor subunits was difficult in the *Plasmodium* mitochondria. Here we report candidates for the membrane anchor subunits of the *Plasmodium* oxidative phosphorylation enzymes. SDH3 and SDH4 of Complex II were identified by using structural fingerprints as probes while subunits *a* and *b* of ATP synthase were identified by BLAST search with proteomics data from other protists. Assignment of the membrane anchors of *Plasmodium* Complex II and ATP synthase will help our understanding of energy metabolism and the development of new antimalarials.

## 2. Materials and methods

### 2.1. Analytical methods

The presence of structural fingerprints (i.e., the heme/quinone-binding motifs) in ORFs shared by *P. falciparum* and *P. y. yoelii* genomes in the TIGR Parasite Database (http://www.tigr.org/tdb/e2k1/pya1/pya1-ortho.shtml/) was examined manually. Database searches using protein sequences were performed with the BLAST service at NCBI (http://www.ncbi.nlm.nih.gov/), GeneDB (http://www.genedb.org/), PlasmoDB (http://plasmodb.org/plasmo/), and TBestDB (http://tbestdb.bcm.umontreal.ca/). Sequences were aligned with ClustalX 2.0 (Larkin et al., 2007) and manual adjustments were made if needed. Transmembrane regions were identified with TMHMM (http://www.cbs.dtu.dk/services/TMHMM/).

## 3. Results and discussion

### 3.1. Evidence for the presence of membrane anchors of Plasmodium Complex II

Mammalian Complex II belongs to type C Complex II (Hägerhäll, 1997) and consists of four subunits and is bound to the matrix side of the inner mitochondrial membrane (Cecchini, 2003). A flavoprotein subunit (Fp, SDH1) and an iron–sulfur subunit (Ip, SDH2) form a soluble heterodimer, which then binds to a membrane anchor *b*-type cytochrome (SDH3/SDH4 heterodimer). SDH1 contains a covalently bound FAD and transfers electrons from succinate to the iron–sulfur clusters in SDH2. Electrons are then transferred to ubiquinone within a binding pocket provided by SDH2 and the SDH3/SDH4 heterodimer (Yankovskaya et al., 2003; Sun et al., 2005; Yang et al., 1998; Horsefield et al., 2006). Bacterial and mitochondrial SDH3 and SDH4 generally consist of three transmembrane helices (TM) each (I–III and IV–VI, respectively) (Yankovskaya et al., 2003; Sun et al., 2005). The quinone/heme-binding motifs, "$RPx_{16}Sx_2HR$" in TM-I and "$Hx_{10}D$" in TM-II of SDH3 and "$Hx_{10}DY$" in TM-V of SDH4 can be identified by sequence comparisons (Figs. 3 and 4). Arg31 (*Escherichia coli* Complex II numbering) in the SDH3 $Sx_2HR$ motif and Asp82 in the SDH4 $Hx_{10}DY$ motif are in close proximity to ubiquinone and could interact with Tyr83 (Yankovskaya et al., 2003). Ser27 in the SDH3 $Sx_2HR$ motif has been shown to be essential for quinone binding (Yang et al., 1998) and is a candidate for hydrogen bonding to the $O_4$ atom of ubiquinone (Horsefield et al., 2006). Tyr83 in the SDH4 $Hx_{10}DY$ motif could hydrogen bond to the $O_1$ atom of ubiquinone and contribute to the binding affinity (Yankovskaya et al., 2003; Horsefield et al., 2006). Examination of the *E. coli* Complex II structure (PDB 1NEK) suggests that the first arginine (Arg9 in *E. coli* SDH3) in the $RPx_{16}Sx_3R$ motif is in the vicinity of Glu186 in SDH1 and Asp106 in SDH2 and may play a structural role through a hydrogen bond network. Histidines in helices II and V (His84 and His 71 in *E. coli* SDH3 and SDH4, respectively) serve as the axial ligands for heme *b* (Yankovskaya et al., 2003; Sun et al., 2005) (Fig. 4A) but are dispensable for assembly and quinone reduction (Tran et al., 2007; Oyedotun et al., 2007).

Earlier, we have cloned and sequenced genes coding for the *P. falciparum* SDH1 and SDH2 by homology probing (Takeo et al., 2000). In contrast to these subunits, *Plasmodium* SDH3 and SDH4 appear to be highly divergent from their mitochondrial orthologs and are not annotated in the current database at NCBI, GeneDB and PlasmoDB. The *P. falciparum* Complex II previously isolated from whole cell lysates was found to be the SDH1/SDH2 heterodimer with an apparent molecular weight of 90 kDa (Suraveratum et al., 2000). The authors claimed that *Plasmodium* Complex II has a much lower $K_m$ (3 μM) for succinate than mammalian enzymes and has the plumbagin-sensitive succinate–quinone reductase activity. However, the concentration (0.2%) of the non-ionic detergent octyl glucoside used for the isolation of *P. falciparum* Complex II was insufficient to solubilize all membrane proteins (i.e., the critical micelle concentration of octyl glucoside is 0.73%). Octyl glucoside likely dissociates the SDH1/SDH2 dimer from the membrane anchors and the aerobic isolation of the SDH1/SDH2 dimer would likely damage the iron–sulfur clusters in SDH2. Thus, the enzyme activities of such preparations need to be carefully examined. Recently, we identified *P. y. yoelii* Complex II as a 135-kDa band by native PAGE followed by activity staining (Kawahara et al., 2009). 2D-PAGE analysis of the Complex II revealed the presence of two small subunits, candidates for *Plasmodium* SDH3 and SDH4. The succinate–quinone reductase activity of *P. falciparum* and *P. y. yoelii* mitochondria (Takashima et al., 2001; Mi-Ichi et al., 2005; Kawahara et al., 2009) and succinate respiration in rodent malaria mitochondria (Uyemura et al., 2000, 2004) support the presence of membrane anchor subunits of Complex II for transferring electron to ubiquinone molecule within the inner mitochondrial membrane.

### 3.2. Identification of Plasmodium Complex II anchor subunits

Protist SDH3 and SDH4 are generally divergent from their orthologs, so conventional BLAST programs using bacterial and eukaryotic sequences as queries failed to identify *Plasmodium* subunits in the current genome database. Recently, we purified Complex II from the parasitic protist *Trypanosoma cruzi* and identified six each of hydrophilic and hydrophobic subunits by protein sequencing (Morales et al., 2009). Supernumerary non-catalytic

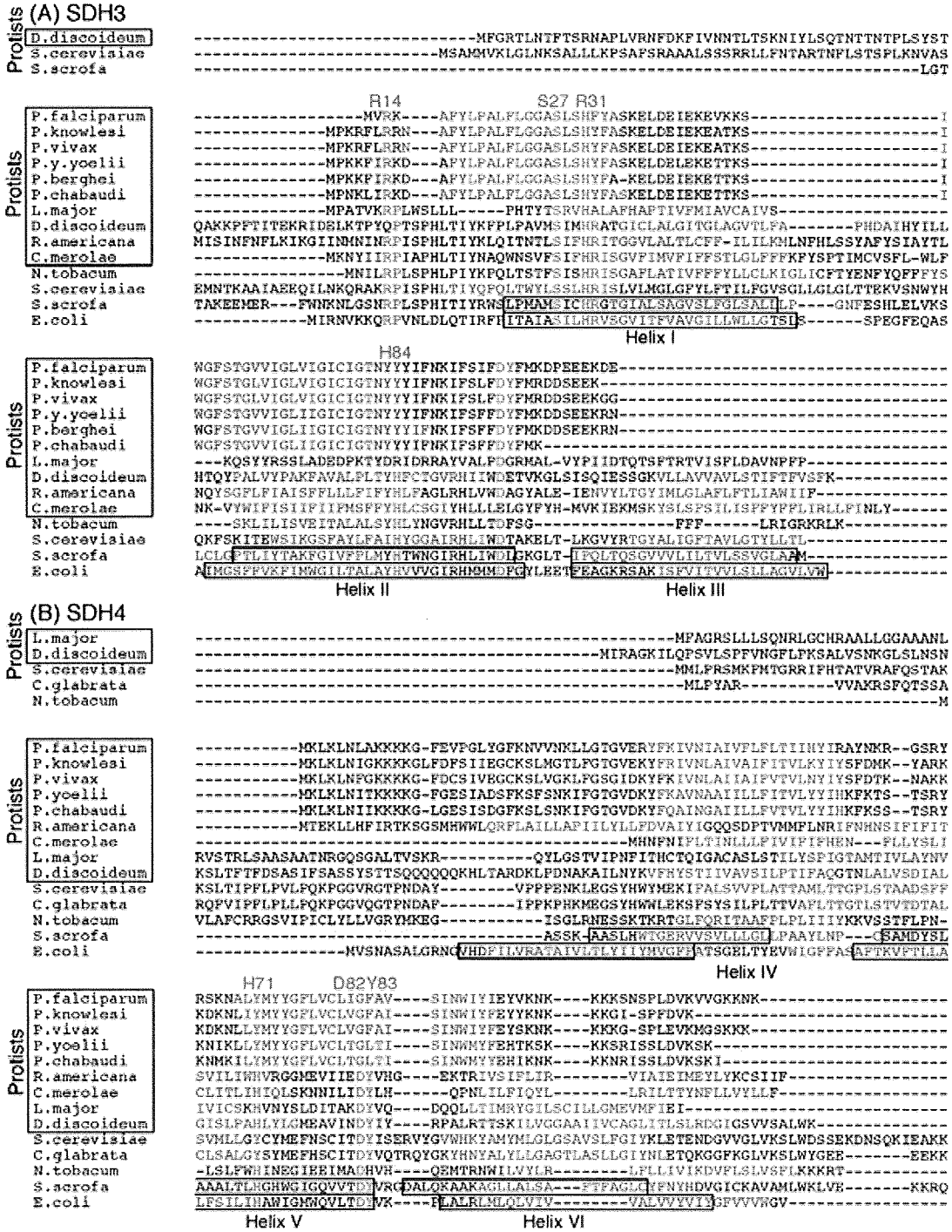


**Fig. 3.** Sequence alignment of SDH3 (A) and SDH4 (B) of *Plasmodium* Complex II. SDH3 and SDH4 sequences (GenBank accession Nos.) used are *P. falciparum* (XP_966100, XP_001347385), *P. knowlesi* (PKH_113810, PKH_080980), *P. vivax* (XP_001616129, XP_001614414), *P. y. yoelii* (XP_731082, XP_726783), *P. berghei* (XP_678526, not available), *P. chabaudi* (XP_742786, XP_738723), *Leishmania major* (XP_848167, XP_001685874), *Dictyostelium discoideum* (XP_643757, XP_642171), *Reclinomonas americana* (NP_044796, NP_044797), *Cyanidioschyzon merolae* (NP_059349, NP_059380), *Nicotiana tabacum* (YP_173376, YP_173457), *S. cerevisiae* S288C (NP_012781, NP_010463), *Candida glabrata* (not used, XP_446226), *Sus scrofa* (1ZOY_C, 1ZOY_D), and *E. coli* (NP_415249, NP_415250). Amino acid residues proposed for binding of ubiquinone and protoheme IX are shown in *red* and transmembrane regions predicted by TMHMM are in *blue*. Residue numbers refer to the *E. coli* SDH3 (SdhC) and SDH4 (SdhD) sequences. Transmembrane helices found in porcine Complex II (PDB 1ZOY) and *E. coli* Complex II (PDB 1NEK) are boxed.

subunits in *T. cruzi* Complex II may have evolved by complementary degeneration of dispersed duplicates (Hurles, 2004) in the Euglenozoa. Among six transmembrane subunits, we identified *T. cruzi* SDH3 and SDH4 on the basis of the presence of the quinone/heme-binding motifs, that are only conserved in these candidates (Morales et al., 2009).

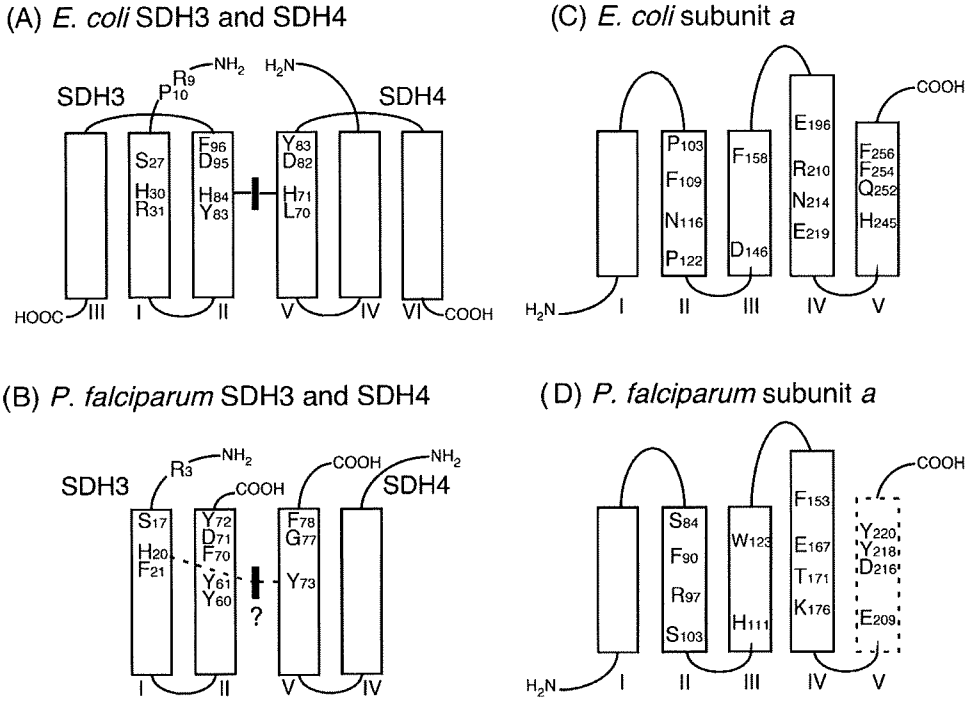


**Fig. 4.** Proposed structures for SDH3 and SDH4 of Complex II and subunits *a* from *E. coli* and *P. falciparum*.

Unlike *T. cruzi* mitochondria, the yield of *Plasmodium* mitochondria and the specific activity of Complex II were very low (Takashima et al., 2001; Mi-Ichi et al., 2005; Kawahara et al., 2009). Therefore, we took an alternative strategy for the identification of *Plasmodium* SDH3 and SDH4. We reexamined manually the sequences of *Plasmodium* membrane proteins for the presence of the quinone/heme-binding motifs of SDH3 and SDH4. Among 3310 ORFs[1] conserved in both *P. falciparum* and *P. y. yoelii* at the TIGR Parasite Database, 15.5% are membrane proteins with putative transmembrane segments, and 2.5% are shorter than 200 amino acid residues, as are the mitochondrial SDH3 and SDH4. From screening based on the number of TMs (1–3), spacing between TMs, conservation in *Plasmodium* spp., and the sequence motifs in transmembrane helices, we identified candidates for *P. falciparum* SDH3 (83 residues, GenBank accession No. XP_966100) and SDH4 (118 residues, XP_001347385) with two putative transmembrane helices (Figs. 3 and 4B, Table 1), which lack helices III and VI, respectively. Sequence identities of *P. falciparum* SDH3 and SDH4 against counterparts in *E. coli* and *Homo sapiens* are 15.7% and 14.3%, respectively, and 23.1% and 21.7%, respectively. An alternative candidate for PfSDH4 (XP_001349911 with one TM) contains the "YHx$_9$DY" motif but TMHMM predicts that this motif is in the C-terminal hydrophilic tail. Orthologs of PfSDH3 and PfSDH4 are present in human malaria parasites *Plasmodium vivax* and *Plasmodium knowlesi* and rodent malaria parasites *P. y. yoelii*, *Plasmodium berghei* and *Plasmodium chabaudi* in the current database[2]. Phylogenetic analysis of amino acid sequences showed that a clade for the membrane anchors of *Plasmodium* and Euglenozoa Complex II is an outgroup of bacterial and mitochondrial SDH3 and SDH4 (Fig. 5).

**Table 1**
Oxidative phosphorylation systems in *P. falciparum*.

| Enzyme | Subunits | GenBank accession no. |
|---|---|---|
| $NDH_2$ | | XP_001352022 |
| Succinate–quinone reductase | SDH1 | XP_001347618 |
| | SDH2 | XP_001350535 |
| | SDH3 | XP_966100 |
| | SDH4 | XP_001347385 |
| Ubiquinol:cytochrome *c* oxidoreductase | Cyt *b* | NP_059668[a] |
| | Rieske FeS | XP_001348547 |
| | Cyt $c_1$ | XP_001348771 |
| | Hinge (QCR6) | XP_001348422 |
| | MPP | XP_001351788, XP_001352201 |
| Cytochrome *c* | Cyc1 | XP_001348211 |
| Cytochrome *c* oxidase | COX I | NP_059667[a] XP_001350328 |
| | COX II | $(2_N)^b$, XP_001348462 $(2_C)^b$ |
| | COX III | NP_059666[a] |
| | COX V | XP_001352148 |
| | COX VI | XP_001352150 |
| | COX VII | CAX64384 |
| | COX VIII | XP_001351632 |
| ATP synthase | ATP1 (α) | XP_001349675 |
| | ATP2 (β) | XP_001350751 |
| | ATP3 (γ) | XP_001349841 |
| | ATP5 (OSCP, δ) | XP_001349828 |
| | ATP16 ($\delta_m$, ε) | XP_001348152 |
| | ATP15 ($\varepsilon_m$) | XP_001349058 |
| | ATP7 (d, p18) | XP_001348820 |
| | ATP6 (*a*) | XP_001347344 |
| | ATP4 (*b*) | XP_001348969 |
| | ATP9 (*c*) | MAL7P1.340 |
| Dihydroorotate dehydrogenase | | XP_966023 |
| NAD(P)-transhydrogenase | | XP_001348682 |

[a] Heterodimeric COX II consist of two degenerated subunits, which retains the *N*- or *C*-terminal functional domain.

[1] Re-examination of the annotation of the *P. y. yoelii* genome on the basis of a detailed analysis of a comprehensive set of cDNA sequences and the liver stage proteome identified a further 510 genes which have orthologs in the *P. falciparum* genome (Vaughan et al., 2008). Analysis of these sequences did not yield any candidates for Complex II SDH3 and SDH4 and ATP synthase subunits *a* and *b*.

[2] The PbSDH3 sequence seems incomplete and the PbSDH4 sequence has not been identified yet at GeneDB. At NCBI, PfSDH3 was identified in *Toxoplasma gondii* and the alternative PfSDH4 was found in other *Plasmodium* species, *T. gondii*, *Babesia bovis*, and *Theileria parva*.

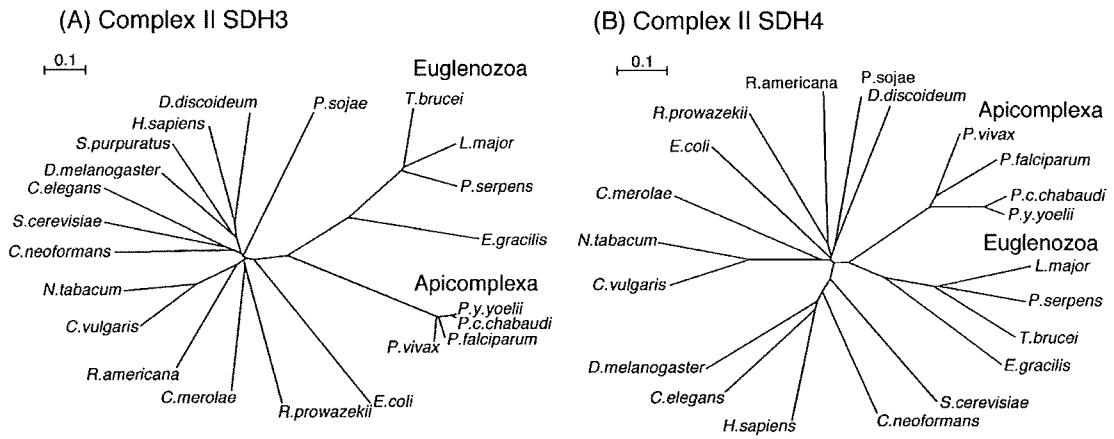


**Fig. 5.** Unrooted phylogenetic trees for SDH3 and SDH4 of Complex II. SDH3 and SDH4 sequences (GenBank accession Nos.) used are *H. sapiens* (NP_002992, NP_002993), *Caenorhabditis elegans* (NP_499283, NP_496369), *Cryptococcus neoformans* (XP_566692, XP_569088), *T. brucei* (XP_845531, XP_823384), *Phytomonas serpens* (CO723838, CO723900), *Euglena gracilis* (EC671331, EC610072), and *Rickettsia prowazekii* (NP_220518, NP_220519). All other sequences are described in the legend to Fig. 3.

### 3.3. Heme and quinone binding sites of Plasmodium Complex II

In *Plasmodium*, SDH3 contains an "$Rx_{13-14}Sx_2HY(F)$" motif in the *N*-terminal region of helix I and a "$YYx_{10}DY$" motif in the *C*-terminal region of helix II, in place of "$RPx_{16}Sx_2HR$" and "$YHx_{10}D$" motifs in other organisms (Figs. 3 and 4). *Plasmodium* SDH4 contains a "$Yx_{10}G$" motif in helix V in place of the canonical "$Hx_{10}DY$" motif (Figs. 3 and 4). Sequence alignments indicate that the tyrosines may substitute

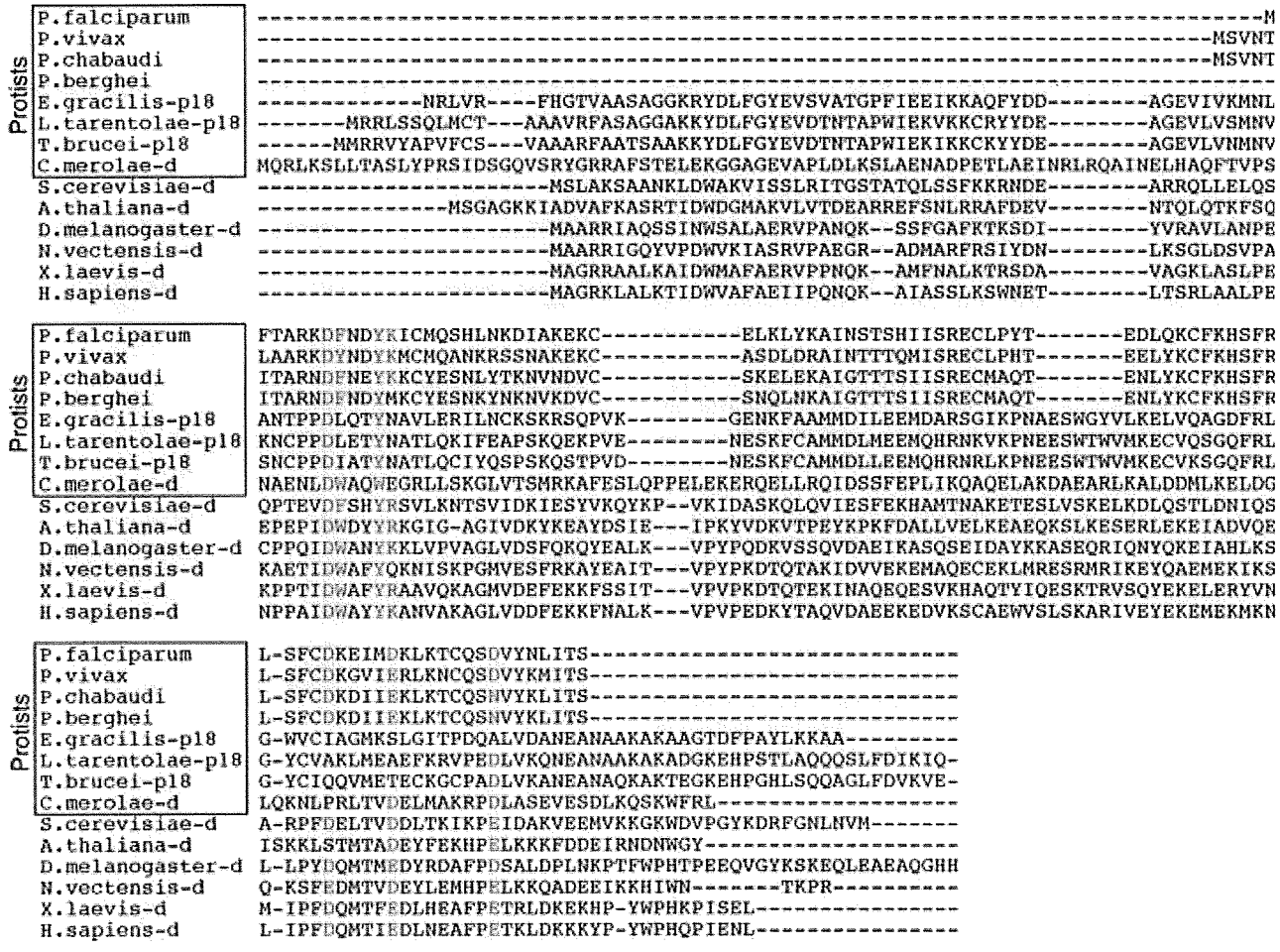


**Fig. 6.** Sequence alignment of subunit *d* (ATP7) of protist ATP synthase. Sequences used (GenBank accession No.) are *P. falciparum* (XP_001348820), *P. vivax* (PVX_117075), *P. c. chabaudi* (PCAS_133570), *P. berghei* (PB001416.02.0), *E. gracilis* (EC671747), *Leishmania tarentolae* (Q25423; p18), *T. brucei* (XP_844845; p18), *S. cerevisiae* (NP_012909), *Arabidopsis thaliana* (NP_190798), *Drosophila melanogaster* (NP_524402), *Nematostella vectensis* (XP_001626831), *Xenopus laevis* (NP_001084746), and *H. sapiens* (NP_006347). *C. merolae* subunit *d* sequence (CMK178C) was obtained at *Cyanidioschyzon merolae* Genome Project.

for Arg in the SDH3 "$Sx_2HR$" motif and histidines as heme ligands in SDH3 and SDH4 (Yankovskaya et al., 2003; Sun et al., 2005). It has been suggested that the role of a heme ligand in helix II (His84 in *E. coli* SDH3) could be replaced by a nearby histidine in the quinone-binding motif "$Sx_2HR$" in helix I (Maklashina et al., 2001). In SDH4 from *Saccharomyces cerevisiae* strain S288C (NP_010463) and rice (NP_001045324), the heme ligand His is substituted by Tyr and Gln, respectively. In catalase (Fita and Rossmann, 1985)


**Fig. 7.** Sequence alignment of subunit *b* (ATP4) of protist ATP synthase. Sequences used (GenBank accession No.) are *P. falciparum* (XP_001349752), *P. vivax* (XP_001613405), *P. berghei* (XP_680022), *P. c. chabaudi* (XP_743670), *Paramecium tetraurelia* (XP_001429993), *T. brucei* (XP_844845), *R. americana* (NP_044805), *Hemiselmis andersenii* (YP_001874763), *D. discoideum* (YP_001604088), *Phytophthora brassicae* (ES285372), *C. merolae* (NP_059355), *S. cerevisiae* (NP_015247), *Marchantia polymorpha* (NP_054459), *A. thaliana* (NP_085524), *D. melanogaster* (Q94516), *N. vectensis* (XP_001635800), *H. sapiens* (NP_001679), *Bradyrhizobium japonicum* (NP_767825), and *E. coli* (NP_418192). Domain structures shown are those proposed for *E. coli* AtpF (Dunn et al., 2000). Transmembrane helices predicted by TMHMM are indicated in *blue* and conserved residues are shown in *red*.

and other hemoproteins Tyr can coordinate the heme and the His-to-Tyr mutant of the yeast SDH3 "YHx$_{10}$D" motif retained half of the enzyme activity and heme content (Oyedotun and Lemire, 1999). In contrast to rhodoquinol–fumarate reductase (type C FRD) from parasitic nematodes (Saruta et al., 1995), menaquinol–fumarate reductase (type D FRD) from *E. coli* lacks heme *b* although membrane anchor subunits FrdC and FrdD have His and Cys, respectively, at the equivalent position of His84 and His71 of *E. coli* SdhC and SdhD, respectively (Hägerhäll, 1997; Cecchini, 2003). Depending on host environments, like *E. coli* FRD, *Plasmodium* Complex II may be able to catalyze both succinate oxidation and fumarate reduction despite *Plasmodium* mitochondria do not have low potential quinones. The presence or absence of the bound protoheme IX in *Plasmodium* Complex II and its enzymatic properties must be tested in future studies using the purified enzyme.

### 3.4. Membrane anchor subunits of Plasmodium ATP synthase

For a long time, it has been assumed that *Plasmodium* mitochondria cannot carry out oxidative phosphorylation (Fry and

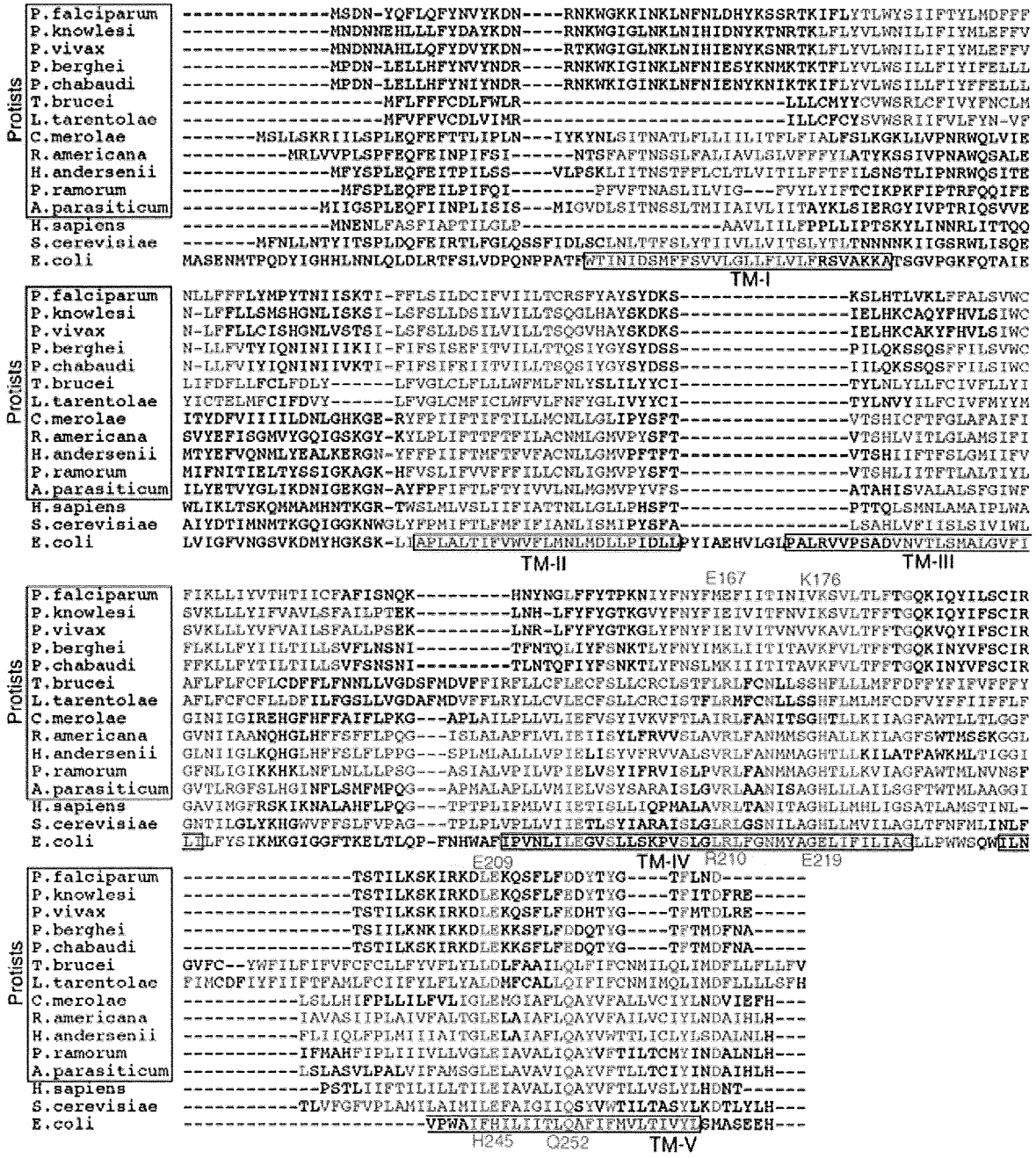


**Fig. 8.** Sequence alignment of subunit *a* (ATP6) of protist ATP synthase. Sequences used (GenBank accession No.) are *P. falciparum* (XP_001347344), *P. knowlesi* (CAQ39459), *P. vivax* (XP_001614365), *P. berghei* (XP_676120), *P. chabaudi* (XP_745940), *T. brucei* (AAA97428), *L. tarentolae* (AAA96695), *C. merolae* (NP_059364), *R. americana* (NP_044804), *H. andersenii* (YP_001874775), *D. discoideum* (NP_050086), *Phytophthora ramorum* (YP_001165346), *Amoebidium parasiticum* (AAN04079), *H. sapiens* (NP_536848), *S. cerevisiae* (CAA24054), and *E. coli* (NP_418194). Transmembrane helices (TM) predicted by TMHMM are indicated in *blue* and those proposed for *E. coli* AtpB (Moore et al., 2008) are boxed. Conserved amino acid residues in TM-IV and -V are shown in *red*.

Beesley, 1991) because of the apparent lack of transmembrane subunits *a* and *b* of the $H^+$-translocating $F_oF_1$-ATP synthase (Carlton et al., 2002; Gardner et al., 2002). However, oxidative phosphorylation in rodent malaria mitochondria (Uyemura et al., 2000, 2004) supports the presence of subunits *a* an *b* of the $F_o$ subcomplex, which serve as the stator in the rotary mechanism (Noji et al., 1997; Fillingame et al., 2000) (Fig. 2), in *Plasmodium* ATP synthase.

Subunits *a* and *b* of protist ATP synthase are also highly divergent from bacterial and eukaryotic counterparts and are frequently not anotated in the database (Seeber et al., 2008). In mitochondrial genomes of land plants and certain protists, ORFs *ymf19* (*orfB*) and *ymf39* are conserved. Based on the sequence similarity and of mass spectrometric analysis, *Ymf19/OrfB* was assigned as subunit ATP8 (A6L) of the sunflower ATP synthase (Sabar et al., 2003). By protein sequencing and mass spectrometric analysis, Ymf39 was assigned as subunit *b* (ATP4 in mitochondria, AtpF in bacteria) in the jakobid *Seculamonas ecuadoriensis* (Burger et al., 2003), and the kinetoplastids *Crithidia fasciculata* (Speijer et al., 1997) and *Leishmania tarentolae* (Nelson et al., 2004). Based on peptide sequences of the *C. fasciculate* ATP synthase subunits, Allen et al. (2004) identified seven subunits of *Trypanosoma brucei* ATP synthase. By using these protist sequences as queries, we identified candidates for 10 subunits of *Plasmodium* ATP synthase with the current database (Table 1). In the mitochondrial ATP synthase, subunits *b* and $\varepsilon$ of bacterial enzymes are split to subunits *b* and *d* and subunits $\delta_m$ and $\varepsilon_m$, respectively. We noticed that ATP16 ($\varepsilon$, $\delta_m$) was mislabeled as ATP15 ($\varepsilon_m$) in *T. brucei* ATP synthase (Allen et al., 2004). Trypanosomatid p18 has been assigned as subunit *b* in previous studies (Nelson et al., 2004; Zíková et al., 2009). It is a hydrophilic nuclear gene product and our sequence analysis indicates that trypanosomatid and euglenid p18s are more closely related to subunit *d* (ATP7) (Devenish et al., 2000) (Fig. 6). As discussed by Burger et al. (2003), subunit *b* is rather featureless except for the locations of its transmembrane helices in the *N*-terminal region (Dunn et al., 2000) and there is no strictly conserved residue throughout species (Fig. 7).

Since the *C. fasciculate* band 3 homolog has four putative transmembrane helices, we tentatively assigned band 3 as subunit *a* (ATP6, AtpB) among four unassigned subunits of *T. brucei* ATP synthase (Allen et al., 2004). Using the *T. brucei* sequence as a query, we identified *Plasmodium* subunit *a* (Fig. 8). The sequence identities of *P. falciparum* subunit *a* with the *E. coli* AtpB (Fig. 4C) and *H. sapiens* ATP6 are 12.9% and 18.8%, respectively. TM-I of *Plasmodium* and *Trypanosoma* spp. showed a high sequence similarity and TM-IV and TM-V are conserved throughout species. Arg210 in transmembrane helix IV (*E. coli* AtpB numbering), which is essential for the proton translocation through the $F_o$ subcomplex (Valiyaveetil and Fillingame, 1977; Fillingame et al., 2000; Moore et al., 2008), is substituted by Glu and Lys in human and rodent malaria parasites, respectively (Figs. 4D and 8). In *E. coli*, second site suppressor mutations of Arg210Gln in TM-IV have been identified as Gln252Arg and Gln252Lys in TM-V (Hatch et al., 1995; Ishmukhametov et al., 2008), indicating close proximity of these conserved residues. Notably, a pair of residues at positions 219 and 245 of *E. coli* subunit *a* are interchanged in mitochondria and the *E. coli* double mutant Glu219His/His245Glu was a slightly functional (Cain and Simoni, 1988). In the malaria parasites, Gln252 is replaced by Asp or Glu and Glu219 and His245 by Lys and Glu, respectively. Despite a lack of Arg210, a set of amino acid substitutions would make the *Plasmodium* subunit *a* functional.

In conclusion, here we identified candidates for six $F_1$ subunits [$\alpha$, $\beta$, $\gamma$, $\delta$ (ATP5, OSCP), $\delta_m$, and $\varepsilon_m$] and four $F_o$ subunits (*a–d*) in *Plasmodium* spp (Table 1). Thus, the *Plasmodium* ATP synthase contains all eight subunits of the *E. coli* ATP synthase ($\alpha_3\beta_3\gamma_1\delta_1\varepsilon$-(=$\delta_m$ *plus* $\varepsilon_m$)$_1a_1b$(=*b plus d*)$_1c_{10?}$) and could carry out a rotary mechanism for ATP synthesis (Noji et al., 1997; Fillingame et al., 2000). Phylogenetic analysis showed that, in contrast to soluble catalytic subunit $\beta$ (not shown), all three membrane anchor subunits, *a*, *b* (Fig. 9) and *c* (not shown), of *Plasmodium* and *Trypanosoma* spp. are divergent from their mitochondrial orthologs. Diversity in membrane anchors of parasitic protist mitochondrial ATP synthase suggests the plasticity in their structures even though they are essential for oxidative phosphorylation. Such variations may modulate or attenuate the function in host environments.

## 4. Conclusion and perspectives

We identified candidates for the membrane anchors of *Plasmodium* Complex II based on the presence of the structural fingerprints and showed sequence divergence from the eukaryotic orthologs. ATPase subunits *a* and *b* of *Plasmodium* were identified based on proteomics data of other protists, and again we found high sequence divergence in the membrane anchors. Our studies

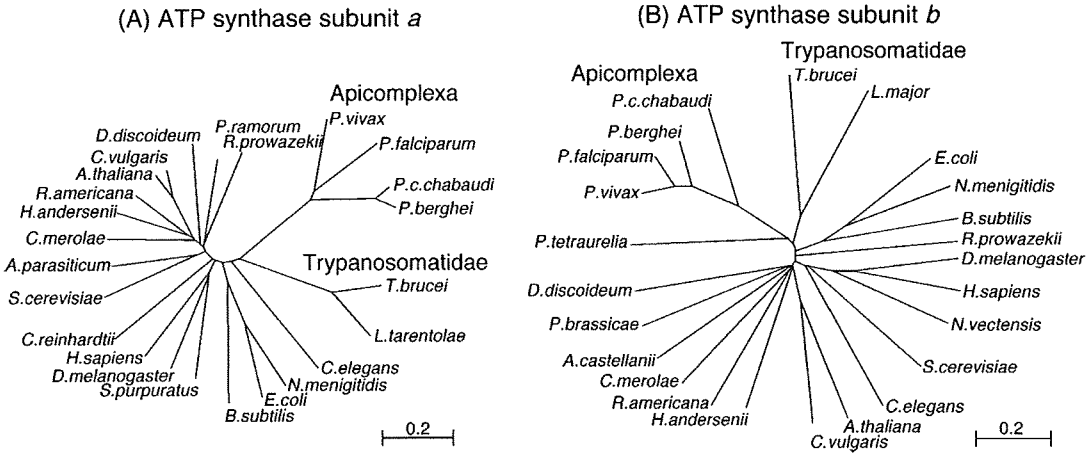


**Fig. 9.** Unrooted phylogenetic trees for subunit *a* (A) and *b* (B) of F-type ATP synthase. Subunits *a* and *b* sequences (GenBank accession Nos.) used are *D. melanogaster* (NP_008281, Q94516), *C. elegans* (NP_006956, NP_497938), *Strongylocentrotus purpuratus* (NP_006971, not available), *A. thaliana* (NP_085569, NP_085524), *Chara vulgaris* (NP_943689, NP_943702), *Chlamydomonas reinhardtii* (XP_001689492, not available), *L. major* (not available, XP_001686628), *Acanthamoeba castellanii* (not available, NP_042558), *R. prowazekii* (NP_220417, NP_220414), *Neisseria meningiditis* (NP_274934, NP_274932), and *Bacillus subtilis* (NP_391568, NP_391566). All other sequences were described in the legends to Figs. 7 and 8. The mitochondrial genomes encode eukaryotic subunits *a* except *C. reinhardtii* and *Plasmodium* spp. and subunit *b* of plants and some protists (*D. discoideum*, *C. merolae*, *R. americana*, and *H. andersenii*).

suggest that *Plasmodium* mitochondria possess all catalytic subunits for Complex II and ATP synthase (Table 1) and are fully capable of oxidative phosphorylation. Our approach is applicable to other membrane proteins although it is rather low throughput. Our assignments should help in understanding parasite energy metabolism.

Recently, diarylquinoline, a new tuberculosis-specific agent, has been shown to bind subunit *c* of ATP synthase (Andries et al., 2005). *Plasmodium* Complex II and ATP synthase could be pathogen-specific targets for new antimalarial agents, because of sequence divergence in membrane anchor subunits. In addition, alternative respiratory enzymes like NDH2 and malate:quinone oxidoreductase (MQO) are absent in mammalian mitochondria and are also promising targets. Since inhibitors for NDH2 are rare and mostly nonspecific (Kerscher, 2000), we screened natural antibiotics and identified gramicidin S and scopafungin as new inhibitors (Mogi et al., 2009). (Saleh et al., 2007) found that 1-hydroxy-2-dodecyl-4(1*H*)quinolone (HDQ), a potent inhibitor for yeast NDH2 (Eschemann et al., 2005), can act as an antimalarial. Even though our compounds were less effective on the *Plasmodium* enzyme than on bacterial enzymes, they may still serve as antimalarials. Such continuing efforts on the screening of natural and synthetic compounds could identify novel and potent drugs against malaria.

## Acknowledgements

This study was supported by a grant-in-aid for scientific research (20570124 to TM) and Creative Scientific Research (18GS0314 to KK) from the Japan Society for the Promotion of Science, and a grant-in-aid for scientific research on Priority Areas (18073004 to KK) from the Ministry of Education, Culture, Sports, Science and Technology, Japan. We would like to thank Dr. B. Lemire (University of Alberta), Dr. G. Burger (University of Montreal), and Dr. S. Sato (National Institute for Medical Research, UK) for critical reading of the manuscript, Dr. M. Llinás (Princeton University), Dr. L. Lasonder, and Dr. H.E. Stunnenberg (Radboud University Nijmegen) for the use of their unpublished results.

## References

Allen, J.W.A., Ginger, M.L., Ferguson, S.J., 2004. Maturation of the unusual single-cysteine (XXXCH) mitochondrial *c*-type cytochromes found in trypanosomatids must occur through a novel biogenesis pathway. Biochem. J. 383, 537–542.

Andries, K., Verhasselt, P., Guillemont, J., Göhlmann, H.W.H., Neefs, J.M., Winkler, H., Gestel, J.V., Timmerman, P., Zhu, M., Lee, E., Williams, P., de Chaffoy, D., Huitric, E., Hoffner, S., Cambau, E., Truffot-Pernot, C., Lounis, N., Jarlier, V., 2005. A diarylquinoline drug active on the ATP synthase of *Mycobacterium tuberculosis*. Science 307, 223–227.

Biagini, G.A., Viriyavejakul, P., O'Neill, P.M., Bray, P.G., Ward, S.A., 2006. Functional characterization and target validation of alternative Complex I of *Plasmodium falciparum* mitochondria. Antimicrob. Agents Chemother. 50, 1841–1851.

Burger, G., Lang, B.F., Braun, H.-P., Marx, S., 2003. The enigmatic mitochondrial ORF *ymf39* codes for ATP synthase chain *b*. Nucleic Acids Res. 31, 2353–2360.

Cain, B.D., Simoni, R.D., 1988. Interaction between Glu-219 and His-245 within the *a* subunit of $F_1F_0$-ATPase in *Escherichia coli*. J. Biol. Chem. 263, 6606–6612.

Carlton, J.M., Angiuoli, S.V., Suh, B.B., Kooij, T.W., Pertea, M., Silva, J.C., Ermolaeva, M.D., Allen, J.E., Selengut, J.D., Koo, H.L., Peterson, J.D., Pop, M., Kosack, D.S., Shumway, M.F., Bidwell, S.L., Shallom, S.J., van Aken, S.E., Riedmuller, S.B., Feldblyum, T.V., Cho, J.K., Quackenbush, J., Sedegah, M., Shoaibi, A., Cummings, L.M., Florensk, L., Yatesk, J.R., Raine, J.D., Sinden, R.E., Harris, M.A., Cunningham, D.A., Preiser, P.R., Bergman, L.W., Vaidya, A.B., van Lin, L.H., Janse, C.J., Waters, A.P., Smith, H.O., White, O.R., Salzberg, S.L., Venter, J.C., Fraser, C.M., Hoffman, S.L., Gardner, M.J., Carucci, D.J., 2002. Genome sequence and comparative analysis of the model rodent malaria parasite *Plasmodium yoelii yoelii*. Nature 419, 512–519.

Cecchini, G., 2003. Function and structure of Complex II of the respiratory chain. Annu. Rev. Biochem. 72, 77–109.

Daily, J.P., Scanfeld, D., Pochet, N., Roch, K.L., Plouffe, D., Kamel, M., Sarr, O., Mboup, S., Ndir, O., Wypij, D., Lavasseur, K., Thomas, E., Tamayo, P., Dong, C., Zhou, Y., Lander, E.S., Ndiaye, D., Wirth, D., Winzeler, E.A., Mesirov, J.P., Regev, A., 2007. Distinct physiological states of *Plasmodium falciparum* in malaria-infected patients. Nature 450, 1091–1095.

Devenish, R.J., Prescott, M., Roucou, X., Nagley, P., 2000. Insights into ATP synthase assembly and function through the molecular genetic manipulation of subunits of the yeast mitochondrial enzyme complex. Biochim. Biophys. Acta 1458, 428–442.

Dunn, S.D., McLachlin, D.T., Revington, M., 2000. The second stalk of *Escherichia coli* ATP synthase. Biochim. Biophys. Acta 1468, 356–363.

Eschemann, A., Galkin, A., Oettmeier, W., Brandt, U., Kerscher, S., 2005. HDQ (1-hydroxy-2-dodecyl-4(1*H*)quinolone), a high affinity inhibitor for mitochondrial alternative NADH dehydrogenase: evidence for a ping-pong mechanism. J. Biol. Chem. 280, 3138–3142.

Fillingame, R.H., Jiang, W., Dimitriev, O.Y., 2000. Coupling of $H^+$ transport to rotary catalysis in F-type ATP synthases: structure and organization of the transmembrane rotary motor. J. Exp. Biol. 203, 9–17.

Fita, I., Rossmann, M.G., 1985. The active center of catalase. J. Mol. Biol. 185, 21–37.

Foth, B.J., Stimmler, L.M., Handman, E., Crabb, B.S., Hodder, A.N., McFadden, G.I., 2005. The malaria parasite *Plasmodium falciparum* has only one pyruvate dehydrogenase complex, which is located in the apicoplast. Mol. Microbiol. 55, 39–53.

Fry, M., Webb, E., Pudney, M., 1990. Effect of mitochondrial inhibitors on adenosine triphosphate levels in *Plasmodium falciparum*. Comp. Biochem. Physiol. B 96, 775–782.

Fry, M., Beesley, J.E., 1991. Mitochondria of mammalian *Plasmodium* spp. Parasitology 102, 17–26.

Gardner, M.J., Hall, N., Fung, E., White, O., Berriman, M., Hyman, R.W., Carlton, J.M., Pain, A., Nelson, K.E., Bowman, S., Paulsen, I.T., James, K., Eisen, J.A., Rutherford, K., Salzberg, S.L., Craig, A., Kyes, S., Chan, M.S., Nene, V., Shallom, S.J., Suh, B., Peterson, J., Angiuoli, S., Pertea, M., Allen, J., Selengut, J., Haft, D., Mather, M.W., Vaidya, A.B., Martin, D.M., Fairlamb, A.H., Fraunholz, M.J., Roos, D.S., Ralph, S.A., McFadden, G.I., Cummings, L.M., Subramanian, G.M., Mungall, C., Venter, J.C., Carucci, D.J., Hoffman, S.L., Newbold, C., Davis, R.W., Fraser, C.M., Barrell, B., 2002. Genome sequence of the human malaria parasite *Plasmodium falciparum*. Nature 419, 498–511.

Hägerhäll, C., 1997. Succinate: quinone oxidoreductases. Variations on a conserved theme. Biochim. Biophys. Acta 1320, 107–141.

Hatch, L.P., Cox, G.B., Howitt, S.M., 1995. The essential arginine residue at position 210 in the *a* subunit of the *Escherichia coli* ATP synthase can be transferred to position 252 with partial retention of activity. J. Biol. Chem. 270, 29407–29412.

Henn, M.W., Schopf, R., Maier, W.A., Seitz, H.M., 1998. The amino acid composition of *Anopheles stephensi* (Diptera: Culicidae) infected with *Nosema algerae* (Microsporida: Nosematidae). J. Invertebr. Pathol. 71, 42–47.

Horsefield, R., Yankovskaya, V., Sexton, G., Whittingham, W., Shiomi, K., Ōmura, S., Byrne, B., Cecchini, G., Iwata, S., 2006. Structural and computational analysis of the quinone-binding site of Complex II (succinate–ubiquinone oxidoreductase). A mechanism of electron transfer and proton conduction during ubiquinone reeuction. J. Biol. Chem. 281, 7309–7316.

Hurles, M., 2004. Gene duplication: the genomic trade in spare parts. PLoS Biol. 2, 0900–0904.

Hyde, J.E., 2005. Drug-resistant malaria. Trends Parasitol. 21, 494–498.

Ishmukhametov, R.R., Pond, J.B., Al-Huqail, A., Galkin, M.A., Vik, S.B., 2008. ATP synthesis without R210 of subunit *a* in the *Escherichia coli* ATP synthase. Biochim. Biophys. Acta 1777, 32–38.

Kawahara, K., Mogi, T., Tanaka, T.Q., Hata, M., Miyoshi, H., Kita, K., 2009. Mitochondrial dehydrogenases in the aerobic respiratory chain of the rodent malaria parasite *Plasmodium yoelii yoelii*. J. Biochem. 145, 229–237.

Kerscher, S.J., 2000. Diversity and origin of alternative NADH:ubiquinone oxidoreductase. Biochim. Biophys. Acta 1459, 274–283.

Larkin, M.A., Blackshields, G., Brown, N.P., Chenna, R., McGettigan, P.A., McWilliam, H., Valentin, F., Wallace, I.M., Wilm, A., Lopez, R., Thompson, J.D., Gibson, T.J., Higgins, D.G., 2007. ClustalW2 and ClustalX version 2. Bioinformatics 23, 2947–2948.

Lasonder, E., Janse, C.J., van Gemert, G., Mair, G.R., Vermunt, A.M.W., Douradinha, B.G., van Noort, V., Huynen, M.A., Luty, A.J.F., Kroeze, H., Khan, S.M., Sauerwein, R.W., Waters, A.P., Mann, M., Stunnenberg, H.G., 2008. Proteomic profiling of *Plasmodium* sporozoite maturation identifies new proteins essential for parasite development and infectivity. PLoS Pathogens 4, e1000195.

Maklashina, E., Rothery, R.A., Weiner, J.H., Cecchini, G., 2001. Retention of heme in axial ligand mutants of succinate–ubiquinone oxidoreductase (Complex II) from *Escherichia coli*. J. Biol. Chem. 276, 18968–18976.

Mi-Ichi, F., Miyadera, H., Kobayashi, T., Takamiya, S., Waki, S., Iwata, S., Shibata, S., Kita, K., 2005. Parasite mitochondria as a target of chemotherapy: inhibitory effect of licochalcone A on the *Plasmodium falciparum* respiratory chain. Ann. NY. Acad. Sci. 1056, 46–54.

Mogi, T., Matsushita, K., Miyoshi, H., Ui, H., Shiomi, K., Ōmura, S., Kita, K., 2009. Identification of new inhibitors for alternative NADH dehydrogenase (NDH-II). FEMS Microbiol. Lett. 291, 157–161.

Moore, K.J., Angevine, C.M., Vincent, O.D., Schwem, B.E., Fillingame, R.H., 2008. The cytoplasmic loops of subunit a of *Escherichia coli* ATP synthase may participate in the proton translocation mechanism. J. Biol. Chem. 283, 13044–13052.

Morales, J., Mogi, T., Mineki, S., Takashima, E., Mineki, R., Hirawake, H., Sakamoto, K., Ōmura, S., Kita, K., 2009. Novel mitochondrial Complex II isolated from *Trypanosoma cruzi* is composed of twelve peptides including a heterodimeric Ip subunit. J. Biol. Chem. 284, 7255–7263.

Nelson, R.E., Aphasizheva, I., Falick, A.M., Nebohacova, M., Simpson, L., 2004. The I-complex in *Leishmania tarentolae* is an uniquely-structured $F_1$-ATPase. Mol. Biochem. Parasitol. 135, 221–224.

Noji, H., Yasuda, R., Yoshida, M., Kinosita, K., 1997. Direct observation of the rotation of $F_1$-ATPase. Nature 386, 299–302.

Oyedotun, K.S., Lemire, B.D., 1999. The *Saccharomyces cerevisiae* succinate–ubiquinone oxidoreductase. Identification of Sdh3p amino acid residues involved in ubiquinone binding. J. Biol. Chem. 274, 23956–23962.

Oyedotun, K.S., Sit, C.S., Lemire, B.D., 2007. The *Saccharomyces cerevisiae* succinate dehydrogenase does not require heme for ubiquinone reduction. Biochim. Biophys. Acta 1767, 1436–1445.

Painter, H.J., Morrisey, J.M., Mather, M.W., Vaidya, A.B., 2007. Specific role of mitochondrial electron transport in blood-stage *Plasmodium falciparum*. Nature 446, 88–91.

Sabar, M., Gagliardi, D., Balk, J., Leaver, C., 2003. ORFB is a subunit of $F_1F_o$-ATP synthase: insight into the basis of cytoplasmic male sterility in sunflower. EMBO Rep. 4, 381–386.

Saleh, A., Friesen, J., Baumeister, S., Gross, G., Bohne, W., 2007. Growth inhibition of *Toxoplasma gondii* and *Plasmodium falciparum* by nanomolar concentrations of 1-hydroxy-2-dodecyl-4(1*H*)quinolone, a high-affinity inhibitor of alternative (type II) NADH dehydrogenases. Antimicrob. Agents Chemother. 51, 1217–1222.

Saruta, F., Kuramochi, T., Nakamura, K., Takamiya, S., Yu, Y., Aoki, T., Sekimizu, K., Kojima, S., Kita, K., 1995. Stage-specific isoforms of complex II (succinate–ubiquinone oxidoreductase) in mitochondria from the parasitic nematode, *Ascaris suum*. J. Biol. Chem. 270, 928–932.

Seeber, F., Limenitakis, J., Soldati-Favre, D., 2008. Apicomplexan mitochondrial metabolism: a story of gains, losses and retentions. Trends Parasitol. 24, 468–478.

Sherman, I.W., 1998. Carbohydrate metabolism of asexual stages. In: Sherman, I.W. (Ed.), Malaria, Parasite Biology, Pathogenesis and Protection. ASM Press, Washington, DC, pp. 135–143.

Speijer, D., Breek, C.K., Muijsers, A.O., Hartog, A.F., Berden, J.A., Albracht, S.P., Samyn, B., van Beeumen, J., Benne, R., 1997. Characterization of the respiratory chain from cultured *Crithidia fasciculate*. Mol. Biochem. Parasitol. 85, 171–186.

Srivastava, I.K., Rottenberg, H., Vaidya, A.B., 1997. Atovaquone, a broad spectrum antiparasitic drug, collapses mitochondrial membrane potential in malarial parasite. J. Biol. Chem. 272, 3961–3966.

Sun, F., Huo, X., Zhai, Y., Wang, A., Xu, J., Su, D., Bartlam, M., Rao, Z., 2005. Crystal structure of mitochondrial respiratory membrane protein complex II. Cell 121, 1043–1057.

Suraveratum, N., Krungkrai, S.R., Leangaramgul, P., Prapunwattana, P., Krungkrai, J., 2000. Purification and characterization of *Plasmodium falciparum* succinate dehydrogenase. Mol. Biochem. Parasitol. 105, 215–222.

Takashima, E., Takamiya, S., Takeo, S., Mi-ichia, F., Amino, H., Kita, K., 2001. Isolation of mitochondria from *Plasmodium falciparum* showing dihydroorotate dependent respiration. Parasitol. Int. 50, 273–278.

Takeo, S., Kokaze, A., Ng, C.S., Mizuchi, D., Watanabe, J.I., Tanabe, K., Kojima, S., Kita, K., 2000. Succinate dehydrogenase in *Plasmodium falciparum* mitochondria: molecular characterization of the *SDHA* and *SDHB* genes for the catalytic subunits, the flavoprotein (Fp) and iron–sulfur (Ip) subunits. Mol. Biochem. Parasitol. 107, 191–205.

Tran, Q.M., Rothery, R.A., Maklashina, E., Cecchini, G., Weiner, J.H., 2007. *Escherichia coli* succinate dehydrogenase variant lacking the heme *b*. Proc. Natl. Acad. Sci. USA 104, 18007–18012.

Uyemura, S.A., Luo, S., Moreno, S.N.J., Docampo, R., 2000. Oxidative phosphorylation, $Ca^{2+}$ transport, and fatty acid-induced uncoupling in malaria parasites mitochondria. J. Biol. Chem. 275, 9709–9715.

Uyemura, S.A., Luo, S., Vieira, M., Moreno, S.N., Docampo, R., 2004. Oxidative phosphorylation and rotenone-insensitive malate- and NADH-quinone oxidoreductases in *Plasmodium yoelii yoelii* mitochondria *in situ*. J. Biol. Chem. 279, 385–393.

Vaidya, A.B., Mather, M.W.A., 2005. Post-genomic view of the mitochondrion in malaria parasites. Curr. Top. Microbiol. Immunol. 295, 233–250.

Valiyaveetil, F.I., Fillingame, R.H., 1977. On the role of Arg-210 and Glu-219 of subunit *a* in proton translocation by the *Escherichia coli* $F_OF_1$-ATP synthase. J. Biol. Chem. 272, 32635–32641.

van Dooren, G.G., Stimmler, L.M., McFadden, G.I., 2006. Metabolic maps and functions of the *Plasmodium* mitochondrion. FEMS Microbiol. Rev. 30, 596–630.

Vaughan, A., Chiu, S., Ramasamy, G., Li, L., Gardner, M.J., Tarun, A.S., Kappe, S.H.I., Peng, X., 2008. Assessment and improvement of the *Plasmodium yoelii yoelii* genome annotation through comparative analysis. ISMB 24, i383–i389.

Yang, X., Yu, L., He, D., Yu, C.A., 1998. The quinone-binding site in succinate–ubiquinone reductase from *Escherichia coli*. Quinone-binding domain and amino acid residues involved in quinone binding. J. Biol. Chem. 273, 31916–31923.

Yankovskaya, V., Horsefield, R., Tornroth, S., Luna-Chavez, C., Miyoshi, H., Leger, C., Byrne, B., Cecchini, G., Iwata, S., 2003. Architecture of succinate dehydrogenase and reactive oxygen species generation. Science 299, 700–704.

Zíková, A., Schnaufer, A., Dalley, R.A., Panigrahi, A.K., Stuart, K.D., 2009. The $F_OF_1$-ATP synthase complex contains novel subunits and is essential for procyclic *Trypanosoma brucei*. PLoS Pathogens 5, e1000436.

Acta Crystallographica Section F
Structural Biology and Crystallization Communications
ISSN 1744-3091

# Overproduction, purification, crystallization and preliminary X-ray diffraction analysis of *Trypanosoma brucei gambiense* glycerol kinase

**Emmanuel Oluwadare Balogun,[a,b] Daniel Ken Inaoka,[a] Yasutoshi Kido,[a] Tomoo Shiba,[a] Takeshi Nara,[c] Takashi Aoki,[c] Teruki Honma,[d] Akiko Tanaka,[d] Masayuki Inoue,[e] Shigeru Matsuoka,[e] Paul A. M. Michels,[f] Shigeharu Harada[g]* and Kiyoshi Kita[a]***

[a]Department of Biomedical Chemistry, Graduate School of Medicine, The University of Tokyo, 7-3-1 Hongo, Bunkyo-ku, Tokyo 113-0033, Japan, [b]Department of Biochemistry, Ahmadu Bello University, Zaria, Nigeria, [c]Department of Molecular and Cellular Parasitology, Juntendo University School of Medicine, Tokyo 113-8421, Japan, [d]Systems and Structural Biology Center, RIKEN, Tsurumi, Yokohama 230-0045, Japan, [e]Graduate School of Pharmaceutical Sciences, The University of Tokyo, Tokyo 113-0033, Japan, [f]Research Unit for Tropical Diseases, de Duve Institute and Laboratory of Biochemistry, Université Catholique de Louvain, Avenue Hippocrate 74, B-1200 Brussels, Belgium, and [g]Department of Applied Biology, Graduate School of Science and Technology, Kyoto Institute of Technology, Sakyo-ku, Kyoto 606-8585, Japan

Correspondence e-mail: harada@kit.ac.jp, kitak@m.u-tokyo.ac.jp

Received 7 September 2009
Accepted 5 January 2010

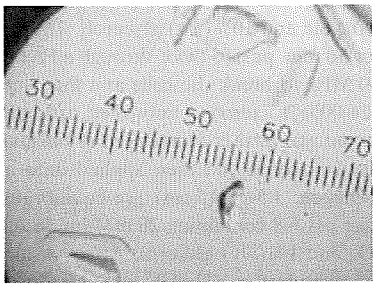




In the bloodstream forms of human trypanosomes, glycerol kinase (GK; EC 2.7.1.30) is one of the nine glycosomally compartmentalized enzymes that are essential for energy metabolism. In this study, a recombinant *Trypanosoma brucei gambiense* GK (rTbgGK) with an N-terminal cleavable $His_6$ tag was overexpressed, purified to homogeneity and crystallized by the sitting-drop vapour-diffusion method using PEG 400 as a precipitant. A complete X-ray diffraction data set to 2.75 Å resolution indicated that the crystals belonged to the orthorhombic space group $P2_12_12_1$, with unit-cell parameters $a$ = 63.84, $b$ = 121.50, $c$ = 154.59 Å. The presence of two rTbgGK molecules in the asymmetric unit gives a Matthews coefficient ($V_M$) of 2.5 Å$^3$ Da$^{-1}$, corresponding to 50% solvent content.

## 1. Introduction

Human African trypanosomiasis (HAT) is a neglected haemoparasitic disease caused by species of the protozoan genus *Trypanosoma* and transmitted by tsetse flies. Over 20 000 new cases are reported annually; it is also a threat to 60 million human lives (World Health Organization, 2006). The human pathogens for the disease are *T. brucei gambiense* and *T. b. rhodesiense*, which cause West and East African trypanosomiasis, respectively, with animals serving as their reservoirs (Njiokou *et al.*, 2006), while the animal pathogens include *T. b. brucei*, *T. vivax*, *T. congolense* and *T. evansi* (Stevens & Brisse, 2004). HAT occurs in two forms: an acute form caused by *T. b. rhodesiense* and a chronic form caused by *T. b. gambiense*. Both agents of the disease present an early haemolymphatic stage and a late meningoencephalitic phase and are deadly at the second stage if left untreated. Unfortunately, only a few drugs are available and problems such as narrow spectrum, treatment failures owing to resistance, high cost and cases of toxicity have been reported (Brun *et al.*, 2001). Therefore, the need to search for new, safer, affordable and more effective drugs with a broader spectrum of action cannot be overemphasized.

Interestingly, the bloodstream forms (BSFs) of these parasites possess several structural and metabolic features that are absent in the mammalian hosts. Such distinctive features, which provide valid drug targets, include compartmentalization of their glycolysis into microbody-like organelles called glycosomes, their sole dependence on glycolysis for their energy needs (Haanstra *et al.*, 2008) and the presence of a rudimentary mitochondrion that houses an indispensable cytochrome-independent alternative oxidase (AOX; Chaudhuri *et al.*, 2006). AOX is not found in the host and its inhibition by salicylhydroxamic acid (SHAM) or ascofuranone (AF) has been reported to cause parasite death as a result of impaired ATP metabolism (Minagawa *et al.*, 1997; Michels *et al.*, 2000; Hannaert *et al.*, 2003; Guerra *et al.*, 2006; Yabu *et al.*, 2006; Singha *et al.*, 2008). In addition, trypanosomes contain a unique glycerol kinase (GK) in their glycosomes. Unlike the host GK, which only catalyses the forward reaction, *i.e.* ATP-dependent glycerol phosphorylation, trypanosomal GK can also catalyze the reverse reaction (Kralova *et al.*, 2000).

Our laboratory has found AF to be an excellent inhibitor of trypanosomal AOX (TAO): its $K_i$ against TAO is 2.38 n*M* (Minagawa *et al.*, 1997) compared with 10 μ*M* for the previously discovered TAO inhibitor SHAM (Njogu *et al.*, 1980). However, *in vitro* and *in vivo* experiments have revealed that AF-induced or SHAM-induced killing of trypanosomes is considerably enhanced when they are co-administered with 5 m*M* glycerol (Fairlamb *et al.*, 1977; Van der Meer & Versluijs-Broers, 1979; Minagawa *et al.*, 1997; Yabu *et al.*, 2006). This synergistic effect of glycerol is most likely to be mediated *via* an expected mass-action-induced inhibition of GK by the added glycerol, thereby blocking the anaerobic ATP generation of glycolysis in the parasites. Unfortunately, this nonphysiologically high concentration of glycerol required for co-administration with AF is toxic to the host. Although GK in conjunction with TAO is thus a promising target for chemotherapy, an effective and selective parasite GK inhibitor has not yet become available.

GK is ubiquitous in archaea, bacteria and eukaryotes, where it belongs to the sugar kinase/heat-shock protein 70/actin superfamily (Hurley, 1996). To date, prokaryotic GKs have been the most widely studied. Of the eukaryotes, structural information is only available on *Plasmodium falciparum* GK, but GK is not essential for growth of the asexual blood stages in this organism (Schnick *et al.*, 2009). Kinetic studies also revealed a striking difference between the GKs of trypanosomes and those of other organisms (Kralova *et al.*, 2000). In *T. b. brucei* GK is encoded by five identical tandemly arranged genes (Colasante *et al.*, 2006) and plays an essential role in the survival of the parasite, especially in the absence of oxygen or in the presence of TAO inhibitors (Minagawa *et al.*, 1997), owing to its ability to catalyze the reverse reaction leading to the production of ATP required by the parasites. One may wonder whether the ability of the trypanosomal GK to catalyze the reverse reaction, in contrast to the human enzyme, is purely a consequence of the compartmentalization in glycosomes of the former or whether structure-based catalytic differences also make a contribution. We therefore perceive the parasite GK to be an interesting subject for structural investigation in terms of fundamental enzymology as well as drug-target exploitation. Here, we report the preliminary X-ray diffraction analysis of GK from *T. b. gambiense*, which may lead us to the design of parasite-specific GK inhibitors that spare the host enzyme. Since *T. b. brucei* TAO has also been crystallized recently (Kido *et al.*, 2010), X-ray structure analysis of both enzymes will aid us in the search for a new generation of chemotherapeutic agents against BSFs.

## 2. Materials and methods

### 2.1. Cloning and expression of TbgGK

Complementary DNA (cDNA) libraries were prepared from stocks of the bloodstream forms of *T. b. gambiense* (IL2343) and *T. b. rhodesiense* (Tbr; IL1501J21) using Toyobo reverse transcriptase. The cDNAs served as templates for the amplification of their GK-encoding genes (*gk*) by PCR using 5′-CACCATGAAGTACGTCGGATCCATT-3′ and 5′-CTACAACTTTGCCCACTTCGTCCTC-3′ as forward and reverse primers, respectively, with *PfuUltra* II Fusion HS DNA polymerase (Stratagene). The amplicons were gel-purified using the Toyobo gel-purification method. Plasmid constructs were obtained by cloning the blunt-ended gene into the pET151/D-TOPO plasmid vector (Invitrogen) by a ligation-independent cloning procedure. Cloning in this vector leads to the addition of an N-terminal tag containing a $His_6$ sequence, a V5 epitope and a tobacco etch virus (TEV) protease cleavage site (for removal of the fused 4 kDa tag) to the expressed recombinant protein.

One Shot TOP10 *Escherichia coli* cells were transformed with the Tbg or Tbr *gk*-pET151/D-TOPO plasmid construct by heat shock. Colonies were grown on Luria–Bertani (LB) plates containing 100 μg ml$^{-1}$ carbenicillin and positive clones carrying the inserted gene were confirmed by colony PCR and selected for liquid culturing in LB media for construct amplification. Plasmid extraction from the cultured TOP10 cells was achieved using a Toyobo MagExtractor kit and was subjected to further confirmation by a combination of nested PCR and digestion with *Nco*I. Gene sequencing using the construct and designed sequencing primers was conducted using the dye-terminator method with an ABI Prism310 genetic analyzer (Applied Biosystems). The nucleotide sequence of *gk* revealed that the Tbg and Tbr GKs were exactly identical at the protein level; hence, Tbg *gk* was picked and used in this study. The recombinant plasmid was transformed into the JM109 (DE3 + pRARE2) *E. coli* strain (Novagen) for protein expression. Colonies of the transformants grown on an LB plate containing 100 μg ml$^{-1}$ carbenicillin and 50 μg ml$^{-1}$ chloramphenicol were selected and grown aerobically in LB medium containing the same concentrations of antibiotics.

The expression conditions were optimized for the amount and the activity of GK in the cytosolic fractions using activity measurements and SDS–PAGE by varying the concentration of the expression inducer isopropyl β-D-1-thiogalactopyranoside (IPTG), the temperature and the post-induction time before transformant harvest. The best yield was achieved with 25 μ*M* IPTG, growth at 293 K and post-induction for 8 h.

### 2.2. Assay of GK activity

The TbgGK activity was assayed using the reverse reaction of TbgGK (glycerol 3-phosphate + ADP → glycerol + ATP). To 1.0 ml of the reaction mixture (1 m*M* EDTA, 5 m*M* $MgSO_4$, 0.5 m*M* $NADP^+$, 50 m*M* glucose, 2 m*M* ADP, 10 m*M* glycerol 3-phosphate and one unit of hexokinase and glucose-6-phosphate dehydrogenase), TbgGK was added at 300 K. Using the ATP produced by TbgGK, hexokinase converts glucose to glucose 6-phosphate and finally glucose-6-phosphate dehydrogenase produces NADPH from glucose 6-phosphate and $NADP^+$. The rate of NADPH accumulation was spectrophotometrically monitored at 340 nm using a Jasco V-660 spectrophotometer.

### 2.3. Purification of recombinant TbgGK

For large-scale preparation, the transformant was grown at 293 K in 10 l LB medium for 8 h after induction and was harvested by centrifugation at 10 000*g*. The *E. coli* pellet was washed twice in 50 m*M* Tris–HCl buffer pH 7.6 containing 0.1 m*M* phenylmethylsulfonyl fluoride (PMSF) and was resuspended in 300 ml lysis buffer [100 m*M* phosphate buffer pH 6.8, 300 m*M* NaCl, 10 m*M* $MgSO_4$, 0.1 m*M* PMSF, 1 mg ml$^{-1}$ lysozyme and 10%(*v*/*v*) glycerol]. The cell suspension was kept on ice for 30 min, passed twice through a French pressure cell operated at 140 MPa to break the cells and then subjected to centrifugation at 26 000*g* to remove unbroken cells and inclusion bodies. The supernatant was further centrifuged at 146 000*g* to remove residual undissolved material and then applied onto an Ni–NTA Agarose column (Qiagen; 1.5 × 15 cm) pre-equilibrated with 100 m*M* phosphate buffer pH 6.8 containing 20 m*M* imidazole, 300 m*M* NaCl, 10 m*M* $MgSO_4$ and 1%(*v*/*v*) glycerol. After washing the column with 100 ml of the same buffer, rTbgGK was eluted with 500 ml of buffer containing a linear gradient of 20–500 m*M* imidazole. Fractions containing active rTbgGK of higher purity as assessed